UNIVERSITAT POLITÈCNICA DE VALÈNCIA

ESCUELA TÉCNICA SUPERIOR DE INGENIERÍA GEODÉSICA CARTOGRÁFICA Y TOPOGRÁFICA

Detection of infant's cranial deformation based on spherical harmonics 3D modeling

Master thesis (*Trabajo Fin de Máster*)

submitted in the academic year 2020-2021 in partial fulfillment of the requirements for the Master's Degree in Geomatics Engineering and Geoinformation (*Máster Universitario en Ingeniería Geomática y Geoinformación*).

Author: Jonas Imanuel Grieb

Supervisor: Prof. José Luis Lerma García

Date of submission: 08.03.2021

Compromiso

El presente documento ha sido realizado completamente por el firmante; no ha sido entregado como otro trabajo académico previo y todo el material tomado de otras fuentes ha sido convenientemente entrecomillado y citado su origen en el texto, así como referenciado en la bibliografía.

Wetzlar, 08.07.2020 J. Grieb

Lugar, fecha Jonas Grieb

Acknowledgments

I would first like to thank my tutor Prof. José Luis Lerma García of the School of Engineering in Geodesy, Cartography and Surveying, Universitat Politècnica de València, for providing me with all necessary advice to write this master thesis. He allowed this thesis to be my own work, but steered me into the right direction whenever he though I needed it. Furthermore, I would like to thank Inés Barbero-García of the Dept. of Cartographic Engineering, Geodesy and Photogrammetry, Universitat Politècnica de València, for providing me with the data sample which was necessary for the completion of this thesis. She also shared with me her valuable opinion and expert knowledge on the topic of the detection of cranial deformation. Finally, I am thankful to my family and friends for all their support. Thank you.

Abstract

3D modeling is increasingly being used for the detection of infant's cranial deformation, where among other methods the deformation has been evaluated by the comparison of the cranium to an ideal cranial shape, represented by a triaxial ellipsoid. This master thesis presents an automatic workflow to model the distances of an infant's cranium to the fitted ellipsoid with spherical harmonics and shows how the resulting spherical harmonic coefficients can be used as indicators for cranial deformation. With the model created in this thesis, the shape of a cranium can be approximated well with a linear combination of the first few spherical harmonic degrees. Furthermore, a possible indicator for plagiocephaly in infant's craniums is identified in the weight which is automatically assigned to a specific spherical harmonic. The developed workflow can be used in automatic classification tasks for the detection of cranial deformations in the future.

Resumen

Las técnicas de modelado 3D se emplean cada vez más en la detección de deformaciones craneales en lactantes. Se ha evaluado la deformación mediante una comparación de la forma del cráneo a una forma ideal representada por un elipsoide triaxial. Este Trabajo Fin de Máster presenta un flujo de trabajo automático que modela las distancias ortogonales del cráneo de un lactante a un elipsoide ajustado y muestra cómo los coeficientes resultantes pueden ser utilizados como indicadores de la deformación craneal. A través del modelo creado en este trabajo, la forma del cráneo puede aproximarse con una combinación lineal de los primeros grados de los armónicos esféricos. Además, es posible identificar como indicador de la plagiocefalia. El flujo de trabajo puede ser utilizado en tareas de clasificación automática de deformaciones craneales en el futuro.

List of Figures

List of Tables

List of abbreviations

CT	Computed tomography
MRI	Magnetic resonance image
PCA	Principal components analysis
RMSE	Root mean square error

Contents

1. Introduction

Cranial deformation is an often occurring medical condition among infants (Aarnivala et al., 2016; Miller and Clarren, 2000). It can lead to complications like craniofacial deformity and may impact neurological development or intracranial pressure (Pindrik et al., 2016). The traditional way to detect and quantify cranial deformations is performed manually under the use of sliding calipers which constitutes a cheap and non-invasive method (Schaaf et al., 2010). A set of well-defined cranial indices which indicate possible cranial deformations exist and can be calculated based on measuring the distance between specific anatomic landmarks on the cranium with the caliper. However, Pindrik et al. (2016) point out a lack of objectiveness and Schaaf et al. (2010) indicate a possible lack of precision due to movements of the infant during the caliper measurement. In order to tackle these problems, recent research works have been proposed to obtain objective measurements and estimations of infant's cranial deformations based on digital imaging and photogrammetric 3D reconstruction of the cranium (Aarnivala et al., 2016; Barbero-García et al., 2017).

The approach from Barbero-García et al. (2017) is particularly important for this master thesis. They developed a lowcost and non-invasive approach to obtain a digital 3D model of the infant's cranium. Barbero-García et al. (2017) describe the ideal cranial shape to be a triaxial ellipsoid. Therefore, they calculate the triaxial ellipsoid which best fits to the obtained 3D data. Then, the mean distance between the ellipsoid and the actually measured cranial shape is proposed as an indicator for cranial deformation. However, this method only allows a global assessment of the deformation and not a localized assessment. Yet, different types of cranial deformation, like plagiocephaly or trigonocephaly, result in very different shapes of the cranium. Therefore, in order to detect which type of deformation is occurring, the cranial surface must be analyzed locally. Based on the idea that the ideal shape of a head is considered to be an ellipsoid, the local variations from the cranium to the ellipsoid should be indicators for the type of cranial deformation. Therefore, the aim of this master thesis is to tackle exactly this question: Do the distances of a cranium to a fitted ellipsoid locally indicate the type of cranial deformation?

In order to analyze the distances from the cranium to its fitted ellipsoid locally, the distances will be modeled with spherical harmonics. Spherical harmonics are "the natural basis functions for describing how a quantity varies across the surface of a sphere" (Wieczorek and Meschede, 2018) and a solution to Laplace's equation. They have been widely applied in different fields of science. They play an important role in Geosciences for the modeling of magnetic and gravitational fields on a planetary scale (Wieczorek and Meschede, 2018). For example, the global model of the Earth's gravitational potential EGM2008, was created as a spherical harmonics model up to degree and order of 2159 and the according coefficients (Pavlis et al., 2012). Also a number of approaches have been described to use spherical harmonics as a shape descriptor for 3D modeling in medical applications (e.g., Gerig et al. (2001), El-Baz et al. (2011)). Since the cranium is approximately a spherical surface, it is assumed in this thesis that this surface can be modeled well with spherical harmonics, too. By modeling the distances from the cranium to the ideal ellipsoid, the information about the cranial deformation should thus be transferred to

the spherical harmonic coefficients. Then, the coefficients can be used as a shape descriptor for the cranium and coefficients which are higher or lower than normal can serve as an indicator to detect the specific type of cranial deformation.

Based on the presented ideas, in this master thesis an approach will be implemented to model the distances from an infant's cranium to the ideal ellipsoid with spherical harmonics. The approach will be tested with a set of 22 available 3D models of infant's craniums. Then, the resulting spherical harmonic coefficients will be analyzed for their potential to serve as an indicator to detect the occurring type of cranial deformation. The thesis is structured as follows: At first, background information will be summarized to provide an overview of the types of cranial deformations treated in this thesis. In that section, related research work on the detection of cranial deformations with 3D modeling will also be presented. Afterwards, the concept of spherical harmonics and how they can be used to model the 3D representation of the cranium will be described. Then, the methodological approach of this master thesis will be explained, which includes a step by step description of how the spherical harmonics model of the cranium is created. Finally, the obtained results will be presented and discussed.

2. Background on cranial deformations

Cranial deformation refers to the untypical deformation of the skull and can be caused by a variety of different factors. Among the various types of cranial deformation, this thesis focuses on four common types which are visible from the outside and can affect infants: brachycephaly, plagiocephaly, scaphocephaly and trigonocephaly. These types of deformations will be explained in more detail in the next section. They can be caused either by craniosynostosis or physical impact. Such physical impact can originate prenatally when the head rests for a prolonged period on a hard part in the womb or, more commonly, originate postnatally from a forced sleeping position (Miller and Clarren, 2000). Deformations from this origin are called deformational plagiocephaly or deformational brachycephaly, also known under the name "flat head syndrom". The other common cause of cranial deformation is craniosynostosis, which is a medical condition that refers to the premature fusion of cranial structures during infancy (Pindrik et al., 2016). Due to this early closing of the cranial structures the head grows irregularly and craniofacial deformations and neurological complications may be the consequence. Craniosynostosis often requires surgical intervention, but on the upside, the current surgical techniques allow an effective and save treatment of craniosynostosis (Mehta et al., 2010). It is estimated to affect about 1 in 2300 live births (Boulet et al., 2008). In contrast, deformational plagiocephaly is reported to may affect up to 48 % of newborns (Miller and Clarren, 2000; Barbero-García et al., 2017). While the latter one is less severe in general, the former one mostly requires surgical intervention. However, it is not always easy to distinguish between deformational plagiocephaly and plagiocephaly caused by craniosynostosis (Johnson and Wilkie, 2011). In the following, the four mentioned common types of cranial deformations in infants will be described briefly. Afterwards, it will be explained which methods are typically used to identify these deformations in infants and related research on this topic will be presented.

2.1. Common cranial deformations

The types of cranial deformations which this thesis focuses on are presented in the following overview (descriptions according to Miller and Clarren (2000) and Johnson and Wilkie (2011)).

1. **Plagiocephaly** is the denomination for an asymmetrical or skewed flattening of one side of the head. It is often the result of a supine sleeping position, but it can also originate prenatally or be the result of craniosynostosis: as the effect of an unilateral coronal synostosis where the coronal sutures of the head close too early or as the effect of a lambdoid synostosis where the bones near the back of an infant's skull close too early.

2. **Brachycephaly** is the denomination for a broad and flattened head shape, which is shorter than usual. In contrast to plagiocephaly the cranium remains symmetric. It also originates often from postnatal physical pressure but it can also be caused by a bicoronial synostosis.

3. **Scaphocephaly/ Dolychocephaly** is the denomination for an extraordinarily long and narrow shape of the head. It is usually caused by sagittal synostosis, i.e., premature closing of the sagittal sutures of the cranium which provokes a longitudinal growth of the head.

4. **Trigonocephaly** is the denomination for the shape caused by metopic synostosis. The metopic suture which is located from the nose up to the sagittal sutures closes too early, thus causing a triangular shape of the forehead.

2.2. Common indices for the detection of cranial deformation

The presented types of cranial deformations are usually detected by measuring the distance between anthropometric landmarks with a caliper and the subsequent calculation of established indices (Schaaf et al., 2010; Wong et al., 2008). Among the most common indices is the so-called cephalic index. It describes the ratio between the maximum breadth and the maximum length of the skull with typical ranges between 0.76 and 0.84 (Johnson and Wilkie, 2011). Thus, it serves well to indicate scaphocephaly (in case of a very small ratio which means that the head is longer than usual) and brachycephaly (in case of a very high ratio which means that the head's width is larger than usual). Furthermore, the frontoparietal index exists which describes the ratio between the minimal width of the frontotemporal part of the skull and the maximum width of the whole skull. Thus, it can serve as an indicator for trigonocephaly if the frontotemporal minimum width is very small in proportion to the maximum width. Additionally to these traditionally in-use indices, Pindrik et al. (2016) describe a new index and provide normative ranges for it: the metopic index. It is similar to the frontoparietal index but it takes a different landmark in the frontal part of the skull as reference, so that it may describe the deformation in case of a trigonocephaly better, according to the authors. As it was mentioned earlier, all these indices are usually based on manual measurements of the cranium under the use of calipers. However, current research focuses on using digital 3D modeling for the measurement of the cranial shape and the calculation of the cranial indices. For this purpose, the head needs to be measured/ scanned and with digital imaging methods a 3D model of the head is created. Then, the positions of the anthropometric landmarks can be derived from the 3D model and used to calculate the cranial indices. However, other research focuses on finding new methods to detect

cranial deformation which make use of the full information that is contained in the 3D model of the cranium. Both approaches will be described in the next section. This thesis follows the latter one and presents a new method for the detection of infant's cranial deformation which will be presented later.

2.3. Related literature

As has been mentioned before, the approach of this master thesis will be based on the approach by Barbero-García et al. (2017). They developed a low-cost smartphone-based method to create a digital 3D model of an infant's cranium with photogrammetry. For this method, a cap with a regular net of targets (Fig. 2a) was placed on the infant's head and scanned with a slow-motion video of a smartphone camera. The resulting image material was used to create a photgrammetric 3D model of the infant's cranium. Even though the images were taken with an average smartphone camera, the resulting 3D model had a similar precision compared to models based on images from a single-lens reflex camera (Lerma et al., 2018). The average difference between the smartphone-obtained models and high-resolution 3D models obtained from Computed Tomography (CT) and Magnetic Resonance Image (MRI) was found to be only 2.1 mm (Barbero-García et al., 2019). The resulting 3D data was used for both general approaches: for the calculation of the cranial indices and for finding new methods to assess cranial deformation. The cranial indices were calculated based on the measurements obtained from the digital 3D model of the cranium. As a new method, Barbero-García et al. (2017) propose the calculation of the orthogonal distances between the actual 3D cranial shape and a fitted ellipsoid. They consider a triaxial ellipsoid as the mathematical surface which best represents the ideal shape of the cranium. Since every head may be different, this ellipsoid needs to be calculated for each cranium individually as the triaxial ellipsoid which is best fitted to the 3D data. Finally, they present the calculation of the orthogonal distances to that fitted ellipsoid as a method "to accurately compute and characterize the deformations" (Barbero-García et al., 2017). As has been mentioned in the introduction, this master thesis aims to take this global assessment of the cranial deformation to a local level.

Other studies focus more on the calculation of the cranial indices presented in the previous section with digital imaging methods: Schaaf et al. (2010) tested the accuracy of anthropometric measurements (like the cephalic index) derived from digital photogrammetry in comparison with traditional manual measurements conducted by professionals. They found a standard deviation of only 7.51 % from the cephalic index derived from photogrammetry in comparison to the manual measurement, and therefore rate the method as reliable. In a similar fashion, Wong et al. (2008) tested the accuracy of measurements of craniofacial landmarks derived from 3D photogrammetric scans against direct manual measurement. A high reliability of the landmark positions from the 3D digital representation and a precision of less than 1 mm was found.

In contrast to the former two studies' focus on the difference between digital photography and manual measurements, Ho et al. (2017) compared the accuracy of 3D photography with computed tomography (CT) scans for the detection of craniosynostosis. CT is considered to be

the gold standard due to its richness of detail, but it comes with the possible risk of radiation. The risk of radiation is especially problematic for infants with craniosynostosis as they require a more frequent 3D scanning of the cranium to monitor the syndrome. Ho et al. (2017) found that 3D imaging is accurate enough for assessing the overall appearance of the cranium and is useful considering that it is less complicated and less invasive than CT. However, they state that the bony structure of the cranium is depicted less optimal by the 3D photogrammetric scan than by the CT scan. Thus, 3D photogrammetry could be less applicable for detecting mild cases of craniosynostosis . Barbero-García et al. (2019) also refer to radiological imaging like the CT method as the gold standard for creating 3D models, and used these as reference data to assess the accuracy of cranial models derived from lowcost smartphone-based photogrammetry. A standard deviation of less than 1.5 mm was measured in the difference between the photogrammetric model and the radiological model, and the mean difference was 2.1 mm. However, Barbero-García et al. (2019) identified that the smartphone-based photogrammetric model overestimated the size of the cranium which was caused by hair and the cap with the photogrammetric targets. The main disadvantage in contrast to the CT scan is, that this method cannot extract information from below the head's surface, as for example the bony structure, which is an important information in the case of craniosynostosis. While CT will remain to be necessary in the case of craniosynostosis, Barbero-García et al. (2019) conclude that the developed 3D photogrammetry method can serve as a routine monitoring technique, especially for deformational plagiocephaly and brachycephaly.

A different approach was taken by Vuollo et al. (2016): Based on the capability of 3D photogrammetry to properly reproduce the shape of the cranium, they developed a new method to detect deformations from the generated 3D data which does not depend on the previously described cranial indices. Thus the method is independent of positioning craniofacial landmarks in the 3D model which is an advantage as it allows the automation of the approach. This method aims to detect deformational brachycephaly or plagiocephaly in infant's heads, the "flat head syndrome". Therefore, based on the flatness property, they performed a kernel density estimate with normal vectors of the 3D model of the head. An accumulation of vectors with the same direction on an otherwise round surface serves as an indicator for flatness caused by deformational brachycephaly or plagiocephaly. In order to further distinguish between these two types of deformations, an asymmetry score was created by comparing the kernel density estimates of the two halves of the head (divided at the sagittal plane) with each other. Deformational plagiocephaly is indicated by an asymmetrical flattening of one side of the head. Based on this, the flattening score and asymmetry score was calculated for a sample of 99 individual 3D models of infant's craniums. Then, the scores were compared with the clinical evaluation of the cranial deformation for each cranium. The results of that study show that the scores correlate with the severity of plagiocephaly or brachycephaly in the sample data, and thus suggest that the created method may serve well as an indicator for these two types of cranial deformation.

Meulstee et al. (2017) proposed another method which takes full advantage of the capabilities of 3D photogrammetry: They performed a principal component analysis (PCA) on a set of 60 3D models representing the shape of healthy infant's craniums. Thus, they could obtain a model

of the mean cranial shape which could be considered as "normal", based on the principal components. Then, they compared this model with the principal components obtained from cranial shapes with scaphocephaly and trigonocephaly. They found the variation in the mean shape to be significant and thus could effectively detect the latter two types of craniosynostosis in infants between 3 and 6 months. A drawback is that the registration of the 3D models obtained from photogrammetry involved a step of manual identification of eight anatomical landmarks on the 3D photographs.

The presented studies show that the 3D modeling of infant's heads by means of photogrammetry and the automatic detection of deformations are actively researched topics at present. The precision of 3D models derived from photogrammetry, even from lowcost smartphone-based photogrammetry, is high enough to allow the detection of cranial deformations. This will not replace CT scan in the future which is required to extract information about the bony structure in case of a diagnosed craniosynostosis, but it may serve for monitoring and follow-up use cases. Several approaches have already been proposed to detect cranial deformations in the 3D models derived from photogrammetric scans, of which the PCA analysis and the kernel density estimate of the vector normals are promising ones. This thesis aims to add a different approach to these methods, by analyzing the potential of spherical harmonics modeling of the distances to the best fitted ellipsoid in order to detect cranial deformations in the derived 3D models of infant's heads. Up to my knowledge, this approach has not been implemented and discussed before.

3. Spherical harmonics

The main idea of this thesis is to use spherical harmonics for the detection of cranial deformation. Based on the assumption that the ideal shape of the cranium can be approximated by an ellipsoid, the aim is to model the distances between the ellipsoid and the real cranial surface with spherical harmonics. Then, the properties of the spherical harmonics model will be investigated to find an indicator for deformation. In order to demonstrate the potential of this, in the following section 3.1 the spherical harmonics and their properties will be described.

3.1. Definition

Many elements in the natural environment are spherical, therefore their investigation requires the use of spherical geometry. As a solution to Laplace's equation, spherical harmonics represent an instrument to model any function which varies across a spherical surface, i.e., as a function to the spherical coordinates (θ, ϕ). A real spherical harmonic $Y_l^m \in \mathbb{R}$ of degree $l \in \mathbb{N}$ and order $m \in \mathbb{Z}$ (where $-l \leq m \leq l$) is defined by Wieczorek and Meschede (2018) as

$$Y_l^m(\theta, \phi) = \begin{cases} \overline{P}_l^m(\cos\phi)\cos m\theta & \text{if } m \geq 0 \\ \overline{P}_l^{|m|}(\cos\phi)\sin|m|\theta & \text{if } m < 0 \end{cases} \tag{1}$$

where θ is the azimutal angle (or longitude), ϕ the polar angle (or colatitude) and $\overline{P}_l^m$ is the

normalized associated Legendre Polynomial given by

$$\overline{P}_l^m(\mu) = \sqrt{(2-\delta_{m0})(2l+1)\frac{(l-m)!}{(l+m)!}P_l^m(\mu)} \tag{2}$$

where $P_l^m(\mu)$ is the associated Legendre Polynomial and δ_{m0} the Kronecker delta function. This definition uses the 4π normalization of the spherical harmonics. Other types of normalization are common in different scientific disciplines, but in this thesis the 4π normalization is utilized as it is used as the default type in Wieczorek and Meschede (2018).

The key in the application of spherical harmonics now is in the linear combination of different types of spherical harmonics. This combination is reached by summing up the result values for all possible spherical harmonics up to a defined maximum spherical harmonic degree l_{max}. Each spherical harmonic Y_l^m(i.e., for each combination of l and m where $l \leq l_{max}$) can then be weighted with a specific coefficient f_l^m in order to approximate an arbitrary function on the sphere. In other words, any real square-integrable function on the sphere can be expressed as the following linear combination of functions on the sphere (according to Wieczorek and Meschede (2018)):

$$SH(\theta, \phi, l_{max}) = \sum_{l=0}^{\infty} \sum_{m=-l}^{l} f_l^m Y_l^m(\theta, \phi) \tag{3}$$

In order to express an arbitrary function or an arbitrary data sample as a sum of spherical harmonics as in Eq. (3), the spherical harmonic coefficients need to be fitted to the data. Since the coefficients are nothing else but weights, this can also be seen as finding the optimal weighting for each spherical harmonics and is an adjustment task. The number of available coefficients which need to bee adjusted is dependent of the chosen l_{max}. The process of adjusting the coefficients f_l^m is called spherical harmonics expansion, or sometimes also referred to as spherical harmonics analysis or spherical harmonics transform. It can be solved in a least squares fashion. The spherical harmonics expansion requires the definition of a l_{max} value. The higher l_{max} is taken, the more detailed the original function can be approximated by the linear combination of spherical harmonics. The reason for this is found in the properties of spherical harmonic which will be explained in the next paragraph.

The properties of the individual spherical harmonics are decisive for their weighting. Among the properties of all spherical harmonics is that they have $l - |m|$ zero crossings in the latitudinal and $2 \cdot |m|$ zero crossings in the longitudinal direction (Wieczorek and Meschede, 2018). Therefore, those spherical harmonics with an order m of zero divide the sphere in zones in the latitudinal direction, as can be observed in Fig. 1a. This type is called zonal harmonics. On the other hand, spherical harmonics whose degree is the same as the absolute value of the order ($l = |m|$) have no zero crossings in the latitudinal direction, which is why they are called sectoral harmonics (see Fig. 1b). All other Y_l^m are called tesseral harmonics as they produce a tesseral net on the sphere which varies both in the latitudinal and longitudinal direction (Fig. 1c). The higher the degree l is, the finer becomes the tesselation. Thus, the higher l_{max} is chosen for the spherical

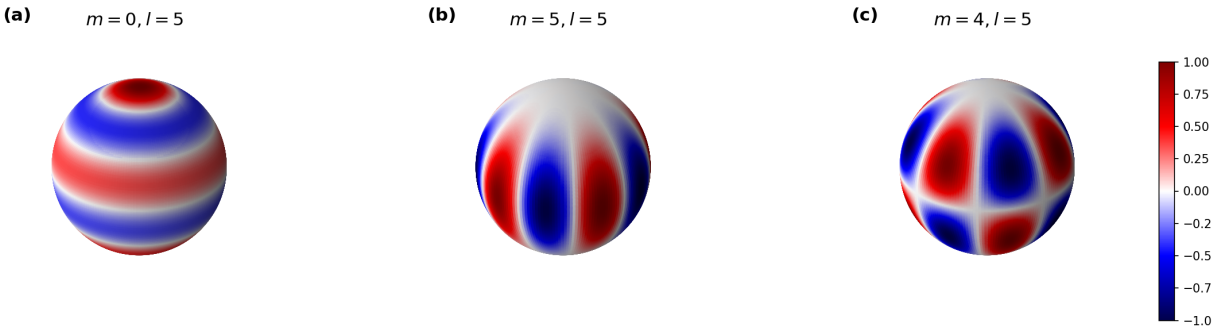

Figure 1: Representation of the function values of typical types of spherical harmonics: (a) zonal, (b) sectoral, (c) tesseral

harmonics expansion, the more detailed becomes the approximation of an original function which is modeled by a linear combination of spherical harmonics and their respective weights as in Eq. (3). A practical example of the application of spherical harmonics expansion and the mode of how they are applied in this thesis will be described in the next section.

3.2. Spherical harmonics for deformation detection

Ducroz et al. (2012) developed an interesting approach for the detection and description of deformation with spherical harmonics, which is similar to the approach taken in this master thesis. They used spherical harmonics expansion to extract and quantify cell shape deformation of amoeboid cells with data derived from biological imaging. They performed a bijective mapping on the derived 3D model of the cell in order to map every position on the cell shape to a unique spherical coordinate. Thus they obtained for every position on the sphere (given by (θ, ϕ)) a unique $x-, y-$ and $z-$ value. Then they performed a spherical harmonics expansion individually for the $x-, y-$ and $z-$ values, i.e., they adjusted the coefficients f_l^m so that the combination of spherical harmonics approximate the respective values. Finally, they analyzed the resulting coefficients and identified patterns in the spherical harmonic coefficients which indicate patterns in the evolution of the cell deformation (Ducroz et al., 2012).

The main difference to the approach by Ducroz et al. (2012) is that in this thesis instead of the $x-, y-$ and $z-$ values, the orthogonal distances to the fitted ellipsoid are modeled with spherical harmonics. To get there, it is required to first calculate the ellipsoid which is best fitted to a cranium and estimate the orthogonal distances from each position on the surface of the cranium to the ellipsoid. The estimation of the orthogonal distances involves the calculation of the closest point on the surface of the ellipsoid for each position on the surface of the cranium. Thus, this step is equivalent to mapping each position to a unique point (θ, ϕ) on the ellipsoid, which serves as the spherical reference surface (see also Fig. 3a). These processing steps will be explained in detail in the methodology section of this thesis. The core idea of modeling the orthogonal distances with spherical harmonics consists in the following: For each point (θ, ϕ) the orthogonal distance d at that point can be modeled as the function value of $SH(\theta, \phi, l_{max}) \approx d$ as in Eq. (3). So, the orthogonal distances are approximated with a linear combination of weighted spherical

harmonics up to a defined maximum spherical harmonic degree l_{max}. In order to understand the potential of the individual spherical harmonics on an infant's cranium, the first spherical harmonic functions are calculated and visualized in the appendix in section A.2. The closest points on the ellipsoid to the positions on the cranial surface roughly correspond to the upper half of the ellipsoid, which is why in the visualizations only the upper half of the spherical harmonic functions of a complete sphere is visible.

By analyzing the function values of the first spherical harmonics mapped to the cranial surface, some interesting observations can be made. For instance, the spherical harmonic of degree $l = 1$ and order $m = 1$ separates the cranium in two hemispheres, a frontal and a dorsal one. This means that this spherical harmonic represents well any function which varies in such a way on a spherical surface, that one hemisphere has mostly positive and the other one mostly negative values. For example, if the differences of the cranium to the ellipsoid are positive in the frontal part of the cranium and negative in the dorsal part, this specific spherical harmonic would be able to represent the variation well. Thus, if the differences are modeled with a combination of spherical harmonic functions as in Eq. (3), then the coefficient f_1^1 corresponding to this spherical harmonic would be large in order to weigh it highly. Analogously, the spherical harmonic function of degree $l = 1$ and order $m = -1$ separates the cranium in two lateral hemispheres (see Fig. 10b). Thus, if the distances to the ellipsoid on one lateral hemisphere are considerably higher in comparison to the other hemisphere, this spherical harmonic function would be weighted with a larger coefficient. It may therefore serve as an indicator of lateral asymmetry of the cranium. In a similar way the spherical harmonic of degree $l = 2$ and order $m = -2$ subdivides the cranium into four longitudinal sectors where each two of them belong to the frontal or dorsal hemisphere of the cranium. Thus f_2^{-2} may represent more precisely if there is lateral asymmetry in the frontal or dorsal part of the cranium.

Based on the potential of the first spherical harmonics which is described above, the following hypotheses are made in order to detect the type of cranial deformation based on the coefficients which are assigned to the individual spherical harmonics:

1. **Brachycephaly** is characterized by an untypical flattening of the back of the cranium. Presuming that this is reflected in the orthogonal distances to ellipsoid in such a way that the distances are smaller in the frontal part of the cranium and larger in the dorsal part, i.e., the difference to the ideal head shape is higher in the dorsal part. Then, the mentioned coefficient of degree $l = 1$ and order $m = 1$ could model well this pattern. Thus, a large value of the corresponding coefficient f_1^1 in the spherical harmonic model could be an indicator for brachycephaly.

2. **Plagiocephaly** is characterized by an asymmetrical flattening at one side of the back of the cranium. Therefore, the mentioned coefficients f_1^{-1} and f_2^{-2} could be indicators for this type of deformation as they model well lateral asymmetry on the cranium. f_2^{-2} has the advantage over f_1^{-1} that it further divides the cranium in a frontal and dorsal part and thus reflects the asymmetry more in detail.

3. **Scaphocephaly** is characterized by the longitudinal growth of the head. This might be reflected well in the spherical harmonic of degree $l = 2$ and order $m = 2$. In Fig. 10e it is shown that this spherical harmonic has large values in the frontal and dorsal part of the cranium, while the lateral parts have small values.

4. The characteristic form caused by **trigonocephaly** is the triangular shape of the forehead. This might be modeled well by the spherical harmonic of degree $l = 3$ and order $m = 3$. As can be observed in Fig. 11e this specific spherical harmonic has small values in the lateral parts of the frontal cranium, whereas in the central frontal cranium the values are positive. By comparing this to Fig. 17 where the orthogonal distances to the fitted ellipsoid of a cranium with trigonocephaly are visualized, it can be appreciated that the pattern is approximately reflected by the mentioned spherical harmonic. Thus, if this spherical harmonic is assigned a greater weight, e.g., a large coefficient f_3^3 in the spherical harmonic model, it could be an indicator for trigonocephaly.

The spherical harmonic functions which are suggested here as possible indicators for cranial deformation are only up to degree $l = 3$. This is because cranial deformation does not affect the cranium punctually in small areas on the cranium but regionally. For example, plagiocephaly and brachycephaly affect the whole dorsal part of the cranium. Trigonocephaly causes the characteristic triangular shape of the whole forehead and scaphocephaly due to the elongated shape of the head affects both, the frontal and the dorsal part of the cranium. As it is described in section 3.1, and as can be observed clearly in the figures in A.2, these regional effects are reflected by spherical harmonics with low degree l. The higher the degree l becomes, the smaller become the tesselerated areas of the function values of the spherical harmonic. As Kakarala et al. (2013) pointed out, one advantage of modeling 3D data with spherical harmonics is that they allow the separation of coarse and fine levels of detail. The mentioned types of cranial deformation affect the coarse structure of the cranial shape, not the fine structure. This coarse structure is reflected in the spherical harmonics of low degrees and thus should be reflected in the coefficients f_l^m with small l. In other words, for the purpose of detection of cranial deformation the information which is contained in the spherical harmonics of higher degrees is not relevant, because these reflect the variation in the small details of the cranial surface, which can naturally be different for every infant. Furthermore, due to the approximately spherical shape of the cranium, it is expected that the distances to the ideal ellipsoid can be modeled well with only a small number of spherical harmonic degrees. This would support the idea that most of the relevant information to detect cranial deformation is reflected in the small degrees l. In order to confirm this, it will also be an aim of this master thesis to show that the distances from a cranium to its ideal ellipsoid (and thus indirectly the cranial shape itself) can be approximated accurately with only a small number of spherical harmonics, i.e., a small maximum degree l_{max}.

4. Objective of this study

This master thesis is based on the following main hypothesis: The orthogonal distances to the best fitted ellipsoid of a cranium can be approximated by performing a spherical harmonics expansion with only a small number of spherical harmonic degrees. Thus, the specific information

about the deformation is transferred to the spherical harmonics coefficients. Therefore it should be possible to detect cranial deformations and possibly classify them into the presented four common types of deformation by analyzing the resulting coefficients.

In order to test the presented hypothesis, the spherical harmonic expansion will be calculated for a sample 22 available 3D representations of infant's craniums. A model will be created which represents the cranium based on a reference ellipsoid and the spherical harmonics. This theoretical model will be referred to in the following as the "spherical harmonics model" (not to be mixed up with the term "3D model" which refers to the digital representation of a specific physical object). The calculation of the model will require the application of several methods which are common in the field of geodesy, for example the calculation of the best fitted ellipsoid, the calculation of the orthogonal distances, and the coordinate conversion on a triaxial ellipsoid. The objective of this study now consists of two goals. First, it will be tested how accurate the created spherical harmonics model of the cranium is with a low maximum number of spherical harmonics. To reach this, the spherical harmonic model will be calculated for every cranium. Then, the cranial shape will be estimated based on the model and compared with the original shape of the cranium. The second goal will be to analyze whether the resulting spherical harmonic coefficients could serve as indicators for the detection of the four different types of cranial deformations on which this thesis focuses on.

5. Data sample

The data sample consists of 22 3D models of infant's craniums, where some of them have cranial deformations. In detail, ten cranial models belong to healthy individuals and twelve possess cranial deformations of different types: One with brachycephaly, four with plagiocephaly, one with a mixed occurrence of brachycephaly and plagiocephlay, four with scaphocephaly and two with trigonocephaly. As mentioned, the data originates from the lowcost smartphone-based photogrammetric method developed by Barbero-García et al. (2017). The software developed based on that method was used to measure the craniums of 22 different infant's and create a 3D model for every cranium. This output constitutes the available data for this thesis. Since Barbero-García et al. (2019) found the accuracy of their developed approach to be approximately 2.1 mm, this is also the accuracy of the available data of this thesis. As it is common for 3D data that was obtained by photogrammetry, the cranial models required a process of registration. As it is described in Barbero-García and Lerma (2019), the data was registered under the use of PCA and three identified tie points. The tie points are positioned centrally over the nose (glabella) and close to the ears (both pre-auricular points). As a result, all available cranial 3D models are comparable with each other. They are centered close to the origin of the three-dimensional Cartesian coordinate system and oriented in such a way that the cranium is longitudinally aligned with the X-axis. The frontal part of the cranium extends over the positive X-axis and the dorsal part over the negative X-axis.

Each cranial model is represented by a 3D triangle mesh. The triangle meshes consist of between 384 to 523 vertices and between 709 and 1012 triangles. The triangles connect the

Table 1: Overview of the available 3D data

ID	Deformation type	Number of vertices	Number of triangles
br1	Brachycephaly	522	1006
nd1	No deformation	522	1006
nd2	No deformation	516	991
nd3	No deformation	516	994
nd4	No deformation	520	1004
nd5	No deformation	523	1006
nd6	No deformation	386	725
nd7	No deformation	478	904
nd8	No deformation	395	743
nd9	No deformation	384	709
nd10	No deformation	392	743
pb1	Brachycephaly + plagiocephaly	518	1000
pl1	Plagiocephaly	522	1009
pl2	Plagiocephaly	519	1001
pl3	Plagiocephaly	521	1005
pl4	Plagiocephaly	523	1011
sc1	Scaphocephaly	515	991
sc2	Scaphocephaly	522	1006
sc3	Scaphocephaly	513	989
sc4	Scaphocephaly	515	994
tr1	Trigonocephaly	404	773
tr2	Trigonocephaly	523	1012

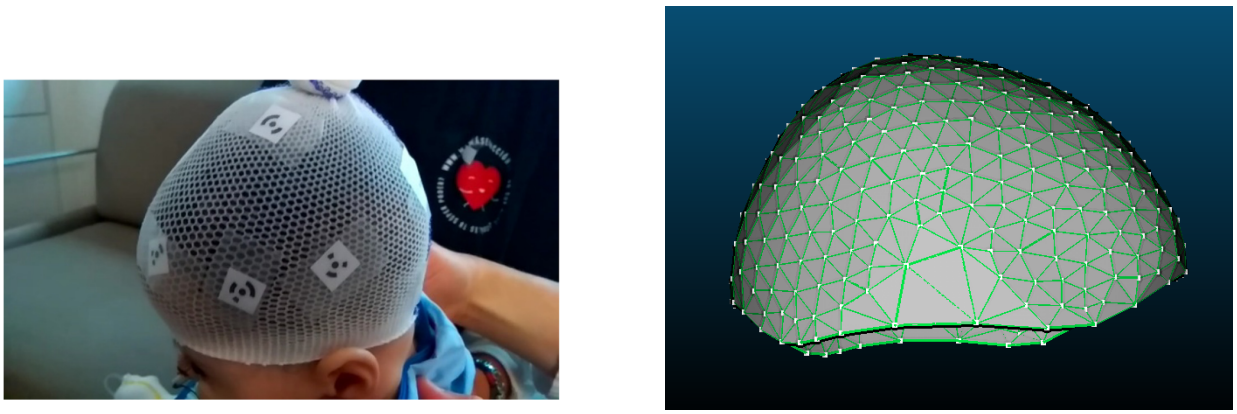

(a) (b)

Figure 2: (a) A cap with targets like this was used by Barbero-García and Lerma (2019) to create the 3D representations of infant's heads which are available for this study (source: Barbero-García and Lerma (2019), ©2018 Elsevier Ltd.), (b) Example visualization of the triangle mesh of pl1

vertices to form a three-dimensional surface which represents each individual cranium. In fact, the facial part of the cranium is left out because the triangle mesh represents only that part of the cranium which is covered by a mask with targets that was used by Barbero-García et al. (2019) (see Fig. 2). All triangle meshes are available in the *Polygon File Format* (PLY). An overview of the individual available data is given in Table 1.

6. Methodology

The approach taken in this project fundamentally consists in the modeling of the distances from the infant's cranium to its best fitted ellipsoid with spherical harmonics. In the first part of this section, the creation of this spherical harmonics model will be explained step by step. The result is a set of spherical harmonics coefficients for every available cranium which will be analyzed in order to detect indicators for cranial deformations. Furthermore, the resulting spherical harmonics model will be evaluated by comparing it to the original cranial model. This is done in order to show that only with a small maximum number of spherical harmonic degrees l_{max} the model approximates the original cranial surface with high accuracy. Therefore, in the second part of this section, it will be explained how the created model is evaluated by comparing the reconstructed cranium with the original one. The approach is designed as an automatic sequence of calculations which are performed on every cranium individually.

6.1. Creation of the model

The basic idea is to model the distances between the cranium and its associated best fitted ellipsoid by spherical harmonics. The best fitted ellipsoid is considered as the ideal cranial shape and is therefore used as the spherical reference surface. To calculate the model for a single cranium the following steps are taken:

1. Calculate the best fitted ellipsoid for the given cranium

2. Estimate the orthogonal distances between the calculated ellipsoid and the real surface of

the cranium

3. Calculate the points on the ellipsoid associated to the orthogonal distances in spherical coordinates (θ, ϕ)

4. Perform a spherical harmonics expansion to obtain the coefficients which are fitted to model the orthogonal distances

In the following, the steps mentioned above will be explained in detail. With the calculation of the spherical harmonic coefficients the modeling process will be completed. Afterwards it will be described how the cranial surface can be reconstructed based on the best fitted ellipsoid and the spherical harmonic coefficients which is necessary for calculating the accuracy in relation to the original 3D model of the cranium.

6.1.1. Best fitted ellipsoid

As was mentioned above, the ideal cranial shape is assumed to be described by a triaxial ellipsoid. This ellipsoid can then serve as a spherical reference surface for the cranium. The point cloud which represents the cranial shape will be projected to this reference surface and the spherical harmonics will be calculated on it. Since every cranium can be different, the reference ellipsoid is calculated for every cranium individually as the ellipsoid which best fits the point cloud data. This is done by a least squares adjustment. The standard equation of a triaxial ellipsoid is

$$\frac{x^2}{a^2} + \frac{y^2}{b^2} + \frac{z^2}{c^2} = 1 \tag{4}$$

where a, b, c are the positive, real-numbered radii of the three axes of the ellipsoid and x, y, z the Cartesian coordinates of a point on the surface of the ellipsoid. This equation is valid for an ellipsoid which is centered at the origin and not rotated, so that the three axes of the ellipsoid are aligned with the axes of the Cartesian coordinate system. However, the ellipsoid which best fits to the point cloud may be shifted in space and rotated about any of the three axes. To describe such an ellipsoid, three more parameters for the vector of the center and three more parameters for the rotation about each of the three axes are needed. Thus, additionally to a, b, c, six more unknown parameters have to be estimated in order to calculate the best fit ellipsoid. The general equation which describes such an ellipsoid with the nine unknowns $[A, B, C, D, E, F, G, H, I]$ is given by Bektas (2015) as

$$Ax^2 + By^2 + Cz^2 + 2Dxy + 2Exz + 2Fyz + 2Gx + 2Hy + 2Iz - 1 = 0 \tag{5}$$

The least squares fitting of a triaxial ellipsoid to a set of points in the 3D space is a common task and has been treated extensively in the literature. The approach which is used in this thesis is described in Bektas (2015) and has been implemented by Judd (2020). The solving of Eq. (5) in a least squares fashion results in a polynomial with given values for $[A, B, C, D, E, F, G, H, I]$. From this polynomial, the parameter values for the radii of the axes, the center and the rotation need to be extracted. To extract these parameters the method described by Judd (2020) was applied. This method returns, as a result, the 3D vector of the center of the ellipsoid $\vec{c}$, the length of the radii of the three axes a, b, c, and a 3x3 rotation matrix R which describes the

rotation of the ellipsoid in the reference system of the input data. The best fitted ellipsoid for a cranium which is defined by these parameters in the reference system of the input data is referred to in the following as E^{data}. However, in the following calculation of the orthogonal distances to the ellipsoid it will be necessary that the ellipsoid is at the origin of the coordinate reference system and not rotated. Therefore, a transformation needs to be applied to the input data, i.e., to the points in the point cloud that describes the cranial surface. This is reached by subtraction of the center $\vec{c}$ and a multiplication with the inverse of the rotation matrix R. The resulting coordinates describe the point cloud in the reference system of the ellipsoid. In contrast to E^{data} which describes the best fitted ellipsoid in the reference system of the input data, the same ellipsoid in its own reference system (e.g., without rotation and centered at the origin) will be referred to as E^{E} in the following.

As it was pointed out by Barbero-García et al. (2017), the ellipsoid fitting needs to be constrained in order to assure that one of the ellipsoid axes matches the longitudinal line from the anterior point to the posterior point of the cranium. This constraint is met by setting the value of E in Eq. (5) to 0, which means that no rotation about the Y-axis is permitted. However, for the purpose of this thesis, which is the local analysis of the deformations, also the rotation about the X-axis and Z-axis constitutes a problem. The best fitted ellipsoid for every cranium is used as reference surface on which the spherical harmonics will be calculated. When the reference ellipsoids are rotated differently this also effects the function values of the spherical harmonics. Thus, the resulting spherical harmonics models for the different craniums would not be comparable with each other. Therefore, the rotation of the best fitted ellipsoid was fully disabled. This means, that also the values of D and F in Eq. (5) were set to zero, so that the axes directions of the fitted ellipsoid would be aligned with the axes of the Cartesian reference system of the input data. The resulting rotation matrix R which is needed for the transformation of the point cloud thus becomes a 3x3 identity matrix and the rotation could be omitted in the implementation of the transformation. It is included in the implementation nonetheless for reasons of completeness and to allow alterations to the workflow in the future. The issue of constraining the rotation of the ellipsoid will be discussed in section 8.

A visualized example of the fitted ellipsoid to one of the available craniums is shown in Fig. 3a. The implemented programming code of the calculation of the best fitted ellipsoid is given in section A.1.1 in the Appendix.

6.1.2. Orthogonal distances to the ellipsoid

In order to model an object with spherical harmonics, it is required to map any element of the object to a unique position on the sphere, defined by its spherical coordinates θ and ϕ. Since the ellipsoid is a spherical surface which can be described by spherical coordinates, it is sufficient to map every position of the surface of the infant's head to the surface of the ellipsoid. This calculation is analog to estimating the orthogonal distances from points in the space to a reference ellipsoid, which is a common procedure in geodesy. The reference ellipsoid in this case is the best fitted ellipsoid E^{data}, calculated as described in the section above. The orthogonal

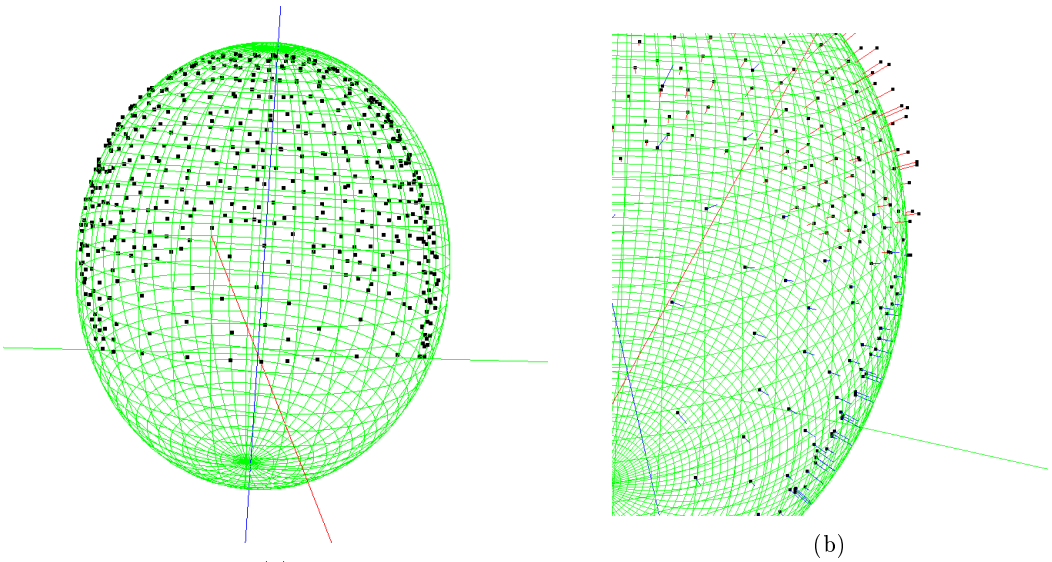

(a) (b)

Figure 3: (a) Visualization of the best fitted ellipsoid for the point cloud of cranium *nd3*, (b) visualization of the orthogonal distances from the points to the fitted ellipsoid, "positive elevations" in red and "negative elevations" in blue

distance of a point on the cranial surface is the closest distance to the surface of the ellipsoid. The strategy of estimating the orthogonal distances that will be applied in this project is based on the method presented in Bektas (2014). Let $O^{data} \in \mathbb{R}^3$ be the point cloud which represents the surface of the infant's head and let the best fitted ellipsoid above be $E^{data} \in \mathbb{R}^3$. Then for every point $P_i \in O^{data}$ the method proposed by Bektas finds the closest point $Q_i \in E^{data}$ which lies on the surface of the ellipsoid. Once that point is known, the orthogonal distance d_i between P_i and the ellipsoid can be calculated as the L2 norm Euclidean distance between P_i and Q_i, i.e., $d_i = ||P_i - Q_i||_2$. The point Q_i is approximated by an initial guess $Q_{i,0}$ and refined in an iterative process until a defined stopping criterion is reached. For the respective equations see Bektas (2014). The stopping criterion in this thesis was defined as that the difference between $Q_{i,j}$ and $Q_{i,j-1}$ is below 0.5 mm (using the L1 norm), so that

$$||Q_i - Q_{i-1}||_1 < 0.5 \tag{6}$$

The orthogonal distances are actually not calculated in relation to E^{data} but to E^E. This means, that beforehand every $P_i \in O^{data}$ is transformed to P_i^E so that it is in the same reference system as E^E with the origin at the center of the ellipsoid. This is reached by a subtraction of the center $\vec{c}$ and a multiplication with the inverse of the rotation matrix R. As a consequence, the orthogonal distances are calculated as the distance between P^E and Q^E. Later, when the cranium will be reconstructed from the model, this transformation needs to be reversed so that the model matches the reference system of the input data.

The result from applying the method to calculate the orthogonal distances is to get a one-to-one projection of every $P_i \in O^{data}$ into E^E. The projected point is the closest point Q_i on the surface of the best fitted ellipsoid. Let the orthogonal distance d_i be defined by $\pm||P_i^E - Q_i^E||_2$. The problem is now that this method only calculates the orthogonal distance to the ellipsoid, but

not whether P is above or below the ellipsoidal surface. However, this information is important because the ellipsoid is considered the ideal head shape and thus serves as the reference surface for the model. As it can be seen in Fig. 3, in some regions the cranial shape is outside of this ellipsoid and in other regions it is inside. So, from the point of view of the ellipsoidal surface the orthogonal distance d_i to P_i is in some regions a positive elevation, and in other regions a negative elevation. This information is needed in order to adequately model the cranial shape as a positive or negative variation from the ellipsoidal surface with spherical harmonics in the following steps. In other words, the information is needed whether the vector of the orthogonal distance at a position on the ellipsoid points towards the exterior (= "positive elevation") or towards the interior of the ellipsoid (= "negative elevation"). In the latter case, keeping in mind that the Euclidean distance always results in a positive d, we need to change the sign of d_i to ensure that $P_i = Q_i + \hat{v}_i \cdot d$, where $\hat{v}_i$ is the unit vector in the direction of the calculated orthogonal distance. This information can be obtained by plugging the Cartesian coordinates (x, y, z) of P_i^E into the left side of the standard equation of the ellipsoid (Eq. (4)). If the result is greater than 1, then P_i is outside of the ellipsoid and nothing is done. But if it is smaller than 1 then P_i lies within the ellipsoid and the sign of d needs to be changed to $-d$. So, the orthogonal distance to the ellipsoid d_i at every point P_i is

$$d_i = \begin{cases} +d_i & \text{if } \frac{x_i^2}{a^2} + \frac{y_i^2}{b^2} + \frac{z_i^2}{c^2} \geq 1 \\ -d_i & \text{if } \frac{x_i^2}{a^2} + \frac{y_i^2}{b^2} + \frac{z_i^2}{c^2} < 1 \end{cases} \tag{7}$$

The programming code which performs the estimation of the orthogonal distances is given in section A.1.2 in the Appendix.

6.1.3. Coordinate conversion on the triaxial ellipsoid

In order to calculate the spherical harmonics as function values on the surface of the ellipsoid E, the spherical coordinates θ and ϕ are needed. This means that the Cartesian coordinates (x, y, z) of every point Q^E need to be converted to ellipsoidal coordinates (θ, ϕ). This coordinate conversion is another common task in Geodesy applications. The relation between the Cartesian coordinates and the spherical coordinates on the triaxial ellipsoid is given in Ligas (2012) by

$$x = (\nu + h) \cdot \cos\phi \cdot \cos\theta \tag{8}$$

$$y = (\nu \cdot (1 - e_e^2) + h) \cdot \cos\phi \cdot \sin\theta \tag{9}$$

$$z = (\nu \cdot (1 - e_x^2) + h) \cdot \sin\phi \tag{10}$$

where ν is the radius of curvature in the prime vertical and e_e^2 and e_x^2 are the first eccentricities squared. However, since Q_E is currently given in Cartesian form and the aim is the conversion to spherical coordinates, the inverse case is needed (also given by Ligas (2012)):

$$\phi = \arctan\left(\frac{(1-e_e^2)}{(1-e_x^2)} \cdot \frac{z}{(1-1-e_e^2)^2 \cdot x^2 + y^2}\right) \tag{11}$$

$$\theta = \arctan\left(\frac{1}{(1-e_e^2)} \cdot \frac{y}{x}\right) \tag{12}$$

For every calculated point Q^E its Cartesian coordinates are converted to spherical coordinates on E according to Eq. [(11),(12)]. The inverse conversion of spherical coordinates to Cartesian coordinates described in the equations [(8),(9),(10)] will be referred to in the following as $E^E(\theta, \phi)$. $E^{data}(\theta, \phi)$ is used to indicate the calculation of the Cartesian coordinates of a given (θ, ϕ) and the subsequent transformation to the reference frame of O^{data} by translation by $\vec{c}$ and rotation by R. This will be needed later for the reconstruction of the original 3D shape based on the spherical harmonics model. The programming code of the coordinate conversion is given in section A.1.3 in the Appendix.

6.1.4. Calculation of the spherical harmonics coefficients

Every $P_i^{data} \in O^{data}$, transformed to P_i^E can now be reconstructed with Q_i^E and the orthogonal distance vector: $P_i^E = Q_i^E + \hat{v_i} \cdot d_i$. However, d_i can also be seen as the spherical harmonic value $SH(\theta_i, \phi_i, l_{max})$ as in Eq. (3) of Q_i^E (expressed in spherical coordinates). In that case, a set of spherical harmonic values d_i and the belonging coordinates on the spherical surface is available. The spherical harmonic expansion consists now in estimating the spherical harmonic coefficients so that the resulting linear combination in Eq. (3) fits to the calculated values of d. To calculate the coefficients, a least squares fitting to the data is performed. This is a common and in case of higher spherical harmonic degrees computationally intensive task. The computation of the coefficients was therefore performed by making use of the *SHTools* library, which was developed by the French Côte d'Azur Observatory and is presented in Wieczorek and Meschede (2018). This library allows the fast calculation of the best fitting coefficients for a given set of coordinates and values with a determined maximum degree. Once the spherical harmonic coefficients are available, the library also allows the rapid evaluation of the inverse case, that means the evaluation of the linear combination of spherical harmonics for a given spherical coordinate (θ, ϕ).

The least squares fitting with the *SHTools* library as described above was applied with the set of points on the ellipsoid Q and the belonging orthogonal distances d as the input data. However, as it was explained in section 3, a further parameter is needed to evaluate Eq. (3): the maximum spherical harmonics degree l_{max}. The higher l_{max} is selected, the more the spherical harmonics model will be able to reflect the details in the input data. In this thesis, for several different craniums the spherical harmonics modeling is performed with different l_{max} values. The results will be presented and discussed in the next section. After passing the described parameters to the *SHTools*, the best fitting spherical harmonics coefficients are calculated and returned. The programming code for the calculation of the coefficients with the *SHTools* library is given in A.1.4.

6.1.5. Reconstruction of the model

With the known spherical harmonic coefficients, the cranial shape can be reconstructed from the surface of the ellipsoid and the orthogonal distance at each position on the ellipsoid which is estimated with the spherical harmonics model. Thus, the original point cloud O^{data} which represents the shape of an infant's cranium can be modeled by:

$$P \in O^{data} = Q_P = (\theta, \phi) = E^{data}(\theta, \phi) + \hat{v}(\theta, \phi) \cdot SH(\theta, \phi, l_{max}) + \varepsilon \tag{13}$$

where Q_P is the projected P on the ellipsoid expressed in spherical coordinates (θ, ϕ), $\hat{v}(\theta, \phi)$ is the unit vector orthogonal to the surface of the ellipsoid at that position , and ε is the error of the model. Furthermore, this model is only valid for that area on the ellipsoid which corresponds to the shape of the cranium projected onto the surface of the ellipsoid. The reconstruction of the cranial shape based on the spherical harmonics model is now the inverse process of how the model was constructed. With the known parameters of the ellipsoid E^{data} and the known spherical harmonics coefficients for a defined l_{max}, for each coordinate in a set of spherical coordinates the following steps are calculated:

1. Conversion to the Cartesian coordinate form of the position on the surface of E^{data}
2. Evaluation of $SH(\theta, \phi, l_{max})$ to obtain the orthogonal distance from E^{data} at the given position
3. Obtain the unit direction vector $\hat{v}(\theta, \phi)$ which is orthogonal to the surface of E^{data} at the given position
4. Evaluate Eq. (13) to obtain the point on the surface of the cranial shape

The steps 1., 2., and 4. of the listing above have already been mentioned before in this thesis and are thus self-explanatory. Step 3. refers to the opposite process of the estimation of the orthogonal distances described earlier. Here, the point on the surface of the ellipsoid is known already and the vector which is orthogonal to the ellipsoid at this position is searched. In order to obtain that vector the normalized gradient vector at this position is calculated. The gradient vector on a triaxial ellipsoid is given in Ligas (2012) as

$$grad(x, y, z) = 2 \cdot \left[\frac{x}{a^2}, \frac{y}{b^2}, \frac{z}{c^2}\right] \tag{14}$$

Therefore, the direction of the orthogonal distance is calculated as the normalized unit vector of the gradient at the position (θ, ϕ), converted to the Cartesian coordinates (x, y, z).

$$\hat{v}(\theta, \phi) = \hat{v}(x, y, z) = \frac{grad(x, y, z)}{||grad(x, y, z)||} \tag{15}$$

With the steps listed above it is now possible to reconstruct the point cloud O^{data} which consists of the vertices of the original cranial shape. For each P_i in O^{data} the corresponding point Q_i on the reference ellipsoid given by (θ, ϕ) is already calculated, as described in section 6.1.2. Now, for every Q_i the spherical harmonics value $SH(\theta, \phi, l_{max})$ at the point is evaluated and the model at the position of P_i is reconstructed as $P_i^{reconstructed}$ as in Eq. (13). $P_i^{reconstructed}$ thus is

an approximation of P_i. This method of reconstructing the original cranium with the spherical harmonics model is referred to in the following as the "reconstruction of the vertices".

In the paragraph above it is explained how the point cloud of the input data can be reconstructed. However, as it is described in section 5, the available input data actually consists in triangulated meshes which represent the surface of an infant's cranium. The point cloud O^{data} is the subset of the vertices included in the triangulated shape, which are connected by the triangles to form a 3D surface. Therefore it is also desirable to reconstruct the cranium as a triangulated surface, based on the spherical harmonics model. This can be reached based on the fact that spherical harmonics are a continuous function on the spherical surface, which can be calculated for every (θ, ϕ). The model given in Eq. (13) though is only valid in that area on the ellipsoid which is covered by the projection of the original triangle mesh to the surface of the ellipsoid. Within this area, the spherical harmonic model can be calculated for any possible position (θ, ϕ). Based on this, the model can be reconstructed by regularly sampling positions (θ, ϕ) on the sphere and calculating the spherical harmonics model for these positions. The regular sample of spherical coordinates was obtained by iterating over a range of azimuth angles $\theta \in [0; 2\pi]$ with a defined step size and for every azimuth iterate over a range of altitude angles $\phi \in [0; \pi]$ with a defined step size. The result is a regularly sampled grid of spherical coordinates where the chosen step size defines the resolution of the grid (see also A.1.5). Each coordinate is then checked whether it is included in the area of the head projected onto the ellipsoid and if yes the spherical harmonics model is evaluated for that position. Finally, the resulting point cloud is triangulated to obtain the spherical harmonics model as a 3D triangulated mesh surface. This method of reconstructing the original cranium with the spherical harmonics model is referred to in the following as the "reconstruction of the surface".

For all 22 available 3D cranial models, at first the described approach to calculate the spherical harmonic coefficients was applied. Afterwards, each model was reconstructed based on the spherical harmonics model as in Eq. (13), once only reconstructing the vertices and once reconstructing the surface of the input cranium.

6.2. Validation of the model

In order to evaluate the developed approach and the model described in Eq. (13), the error of the resulting model is estimated for the available data. The error can be extracted from the distance between the original 3D shape of the cranium and the reconstructed one based on the spherical harmonics model. The distance between both is punctually measured at different positions. The error is then estimated as the root mean square error (RMSE) of all distances measured at the different points. However, as explained earlier there were two different methods applied to reconstruct the 3D model with spherical harmonics: one method where the spherical harmonics are only evaluated at the same points which belong to the input data, and the other method where the spherical harmonics are evaluated on a regularly sampled grid. Analogously, two different methods to measure the mean distance between the original model and the reconstructed model were carried out. The straightforward method is to measure the distance between the points

in the original input data and the corresponding points which were reconstructed based on the spherical harmonics model. This method is useful to measure how well the spherical harmonics model adjusts to the input point cloud. However, since the input data is a triangulated mesh and thus a 3D surface, it is also desirable to test how well the spherical harmonics model adjusts to that surface. This is measured by the second method, where the distance between both models is measured at regularly sampled positions on the spherical surface. In the following, both methods will be explained more in detail.

6.2.1. Distance between the original points and the reconstructed points

As it is described in section 6.1.5, the straightforward method of reconstructing the 3D model with the spherical harmonics model is by calculating for every point P_i the corresponding point $P_{i,reconstructed}$. The error ε is then obtained as the Euclidean distance between P_i and $P_{i,reconstructed}$. The RMSE of the whole model in relation to the original cranial model is thus calculated as

$$RMSE = \sqrt{\frac{1}{n} \cdot \sum_{i=0}^{n} ||P_i^{data} - P_i^{reconstructed}||^2} \tag{16}$$

where n is the number of vertices P in the input triangle mesh of the cranium. In other words, for every point in the input point cloud which represents the cranium, the distance to its corresponding point in the spherical harmonics model is calculated. The overall error is estimated as the RMSE of all distances between the corresponding points. This method of estimating the error was only applied to the reconstructed vertices. The result of this is applied to all available data is shown in Fig. 4a.

6.2.2. Distance between the triangle meshes

The second method to evaluate the distance between the spherical harmonics model and the original 3D model, measures the distance between the actual triangulated meshes in every direction. This is implemented based on a ray casting approach. Ray casting is a method originating from the field of computer graphics where virtual ray lights are cast and their intersections with objects are measured to visualize the objects in the space (Roth, 1982). Here, ray casting refers to a simple line intersection technique in the 3D space. A linear ray is cast from an originating position in all directions and the position where it intersects with the surface of another object in the 3D space is calculated. Considering the approximately spherical shape of both, the cranial 3D model and the spherical harmonics model, a ray cast from the center of the models to a certain direction must intersect with both of the 3D models. The distance between both intersection points can be considered approximately as the distance between both models at this position. Such a ray casting is applied from the center of the ellipsoid E^{data} towards all directions. In every direction where an intersection with both models exists, the distance between both intersection point is measured and the mean of all distances is estimated as the mean distance between both 3D models.

In order to cast a ray in every direction, a virtual sphere is created which consists of a list of regularly sampled azimuth and altitude angles. They are sampled in the same way like the sampling of spherical coordinates as described in section 6.1.5 (see also A.1.5 in the appendix). By converting the spherical coordinate to a Cartesian coordinate, a vector in the direction of the corresponding position on the sphere is obtained. By applying this to all combinations of azimuth and altitude, vectors pointing into all directions are obtained, which are used to test the intersection of the triangulated meshes. The mean distance between the original and the reconstructed mesh is then obtained by:

$$RMSE = \sqrt{\frac{1}{n} \cdot \sum_{i=0}^{n} ||S_i^{data} - S_i^{reconstructed}||^2} \tag{17}$$

where n is the number of sampled coordinates on the unit sphere (θ_i, ϕ_i) which is converted to the Cartesian space where it represents a direction vector, and S_i are the intersection points of the triangulated meshes with the straight line in the direction of that vector.

6.3. Programmatical implementation

The presented method which was developed in this master thesis project has been fully implemented in the Python programming language. Python was chosen for several reasons. First, it is a complete, high-level programming language, which allows operations required for this project like the reading and writing of files, numerical calculations and visualization. Second, due to its high popularity and active community there are many libraries available. Several of these libraries have been used in this project, particularly the libraries NumPy and pyshtools. Numpy provides all the necessary operations to perform numerical operations. pyshtools provides Python bindings to the Fortran-based *SHTools* package which allows fast and accurate spherical harmonic expansions and analysis for geoscience applications. Third, Python was chosen because thus it integrates well with the work of Barbero-García et al. (2017). Their smartphone-based method for the analysis of cranial deformations makes also use of the Python technology. The output of their method is a 3D-model of the infant's cranium, which constitutes the input of the method developed in this thesis. By making use of the same programming language it will be easier to combine the approach developed in this thesis with Barbero-García et al.'s method into a single workflow in the future if desired.

Besides NumPy and pyshtools, the library open3d was used in the implementation as it facilitates the reading and writing of files containing 3D models in the PLY format. It was also partly used for the visualization whereas the other rendered visualizations of the cranial 3D models were carried out with the software CloudCompare. Furthermore, the Python library VTK was used to perform the ray casting calculations. VTK is an open source toolkit for 3D computer graphics operations and therefore its use accelerates the performance of the ray casting calculation considerably.

7. Results

The proposed approach based on spherical harmonics was implemented with programming code so that the spherical harmonics model could be calculated for each cranium in the available data in an automatic way. For every cranium, the spherical harmonics expansion was performed with a series of different l_{max} values, starting with $l_{max} = 1$ up to $l_{max} = 15$. For every resulting spherical harmonics model of every cranium, the accuracy of the model was measured by calculating the distance between the original and the reconstructed cranium with the two methods of distance measuring. Also, for every model the calculated spherical harmonic coefficients were stored and analyzed. In the following, at first the results regarding the accuracy of the model will be presented. Afterwards, the resulting spherical harmonic coefficients will be explained.

7.1. Distance between the original and the reconstructed cranial models

The RMSE of the spherical harmonics model in relation to the original cranial model is for most of the craniums between 2 and 2.5 mm at the smallest number of spherical harmonics degrees ($l_{max} = 1$). With an increasing l_{max} the RMSE decreases and from an l_{max} of 8 and upwards converges towards zero. This general trend can be observed in Fig. 4a. By evaluating the RMSE on the input vertices, it stands out that the RMSE of one cranium with trigonocephaly (tr2) at $l_{max} = 2$ is higher than 2, whereas all other craniums show an RMSE of lower than 2 at the same l_{max}. This means that the cranium tr2 cannot be modeled so well with spherical harmonic degrees up to 2. From $l_{max} = 3$ onward, the RMSE of tr2 falls in the same range as the other craniums. However, as can be seen in Fig. 4b, an exceptionally high RMSE of tr2 at $l_{max} = 2$ is not existent in the RMSE evaluated on the reconstructed triangle shape. This will be discussed again later.

It is noticed that the error of the spherical harmonics model is quite similar for the different craniums inasmuch as no group of craniums shows exceptionally low or high RMSE values in relation to the other groups. Especially the RMSE of healthy craniums and of craniums with scaphocephaly is very similar. For low l_{max} values of up to 3, the RMSE is actually lower for some plagiocephaly and brachychecphaly craniums than for healthy craniums (see Fig. 4). But the differences between the measured RMSE values are small and this is only observed for some singular craniums and not for the whole class. Furthermore, when the RMSE is evaluated on the reconstructed shape, one healthy cranium and one with trigonocephaly (in this case it is tr1) have a clearly higher RMSE than the others (see Fig. 4b). It is noticeable that the RMSE of these two craniums is in the same range as for the other craniums at low l_{max} values, but they stand out at l_{max} values of 4 and higher. Moreover, at l_{max} values of 12 and higher the measured RMSE begins to increase again. In individual tests the developed approach was also performed for some craniums with very high spherical harmonic degrees ($l_{max} = 30, l_{max} = 50$). The RMSE of the resulting models was evaluated on the vertices and also on the reconstructed shape. While the difference between the vertices of the input model and the reconstructed vertices was 0, the resulting reconstructed shape lead to partly absurd results. The higher l_{max} was chosen, the more unstable became the reconstruction of the model at spherical points (θ, ϕ) which were not

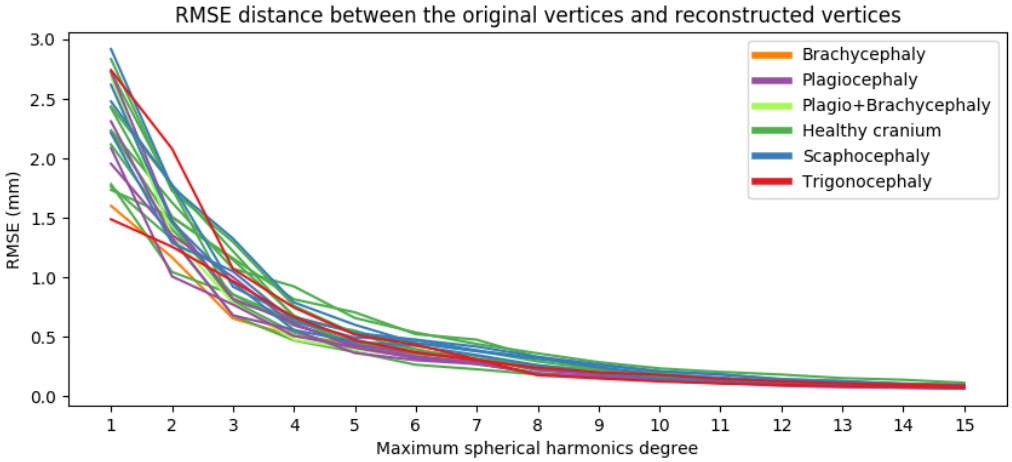

(a) RMSE measured at the input vertices

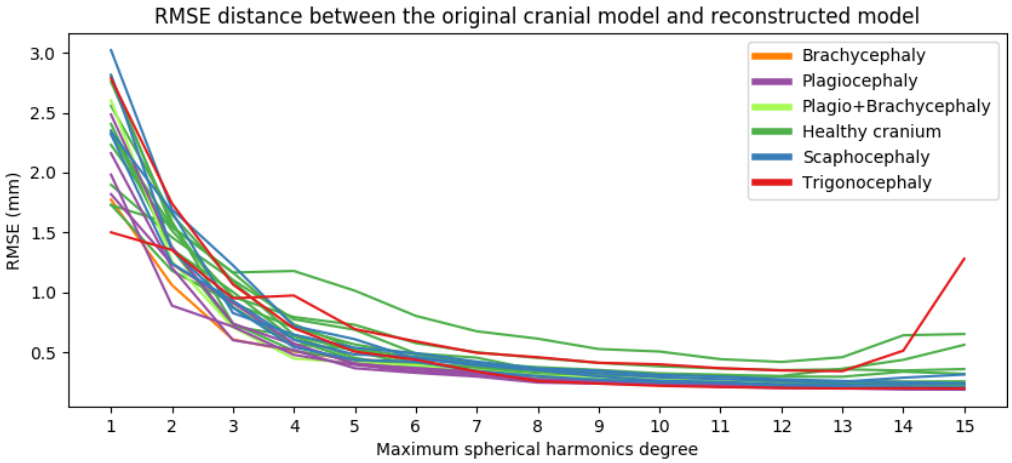

(b) RMSE measured with raycasting on the reconstructed shape

Figure 4: Error of the spherical harmonics model for the available data at different l_{max}

included in the input data.

7.2. Resulting spherical harmonic coefficients

The resulting spherical harmonic coefficients of all craniums were manually analyzed in order to find indicators which allow the detection of the type of cranial deformation. While the coefficient f_2^{-2} was found as a possible indicator for plagiocephaly and f_3^3 for trigonocephaly, no coefficients were found which distinguish the classes brachycephaly and scaphocephaly well from the others. A focus was put on the coefficients of low spherical harmonic degrees because they model the coarse structure of the cranium. An exemplary overview of all calculated coefficients at $l_{max} = 4$ for all craniums is provided in Table A.4.

Scaphocephaly and **brachycephaly**: Among the analyzed spherical harmonic coefficients f_l^m, no coefficients were found which might serve as an indicator for these two types of cranial deformation. An example of this is given in Fig. 5. In this figure the resulting coefficient f_2^2,

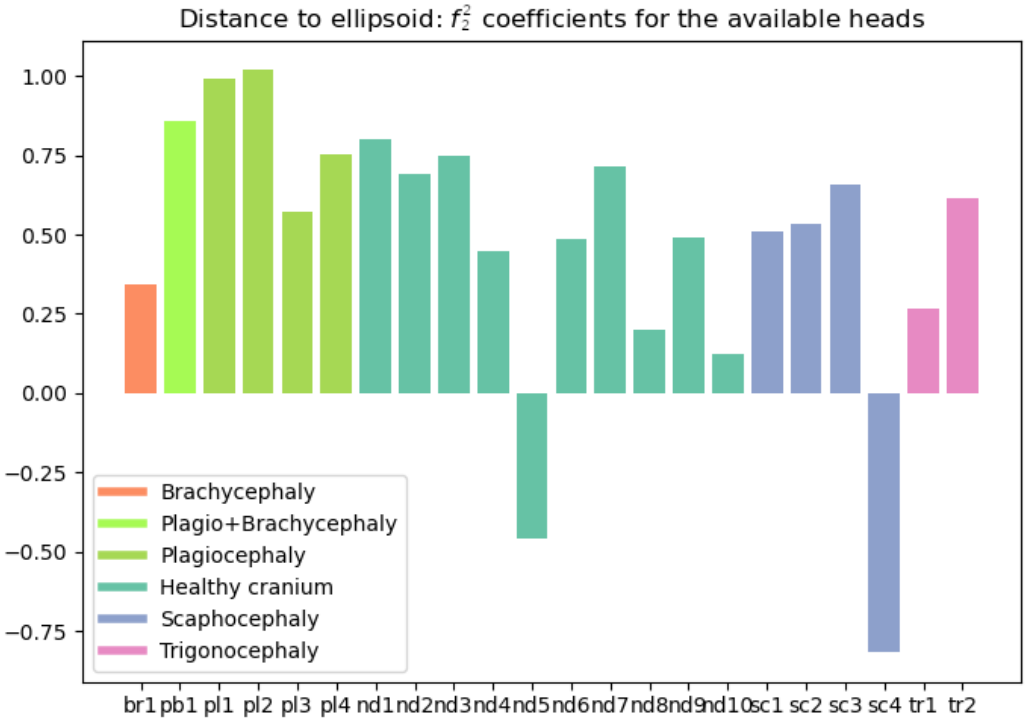

Figure 5: The coefficient of degree $l = 2$ and order $m = 2$ for the available heads, calculated at $l_{max} = 3$.

which has been hypothesized as a possible indicator in section 3.2, is displayed for all craniums. As can be observed in the figure, the coefficients for craniums with scaphocephaly and brachycephaly are just in the same range as for healthy craniums.

Trigonocephaly: No coefficient was identified which distinguishes well the two available craniums with trigonocephaly from the other craniums. However, one of the two, the cranium *tr2*, has a high coefficient at degree $l = 3$ and order $m = 3$. This coefficient f_3^3 also has been hypothesized as a possible indicator for trigonocephaly in section 3.2. As can be observed in Fig. 6, this pattern exists when the spherical harmonics expansion was calculated with $l_{max} = 3$ as well as with $l_{max} = 4$. In both cases, the f_3^3 calculated for *tr2* has the highest value in comparison to the other craniums, especially in comparison to the group of healthy craniums.

Plagiocephaly: The coefficient with degree $l = 2$ and order $m = -2$ was identified as the coefficient which best distinguishes the class of craniums with plagiocephaly from the others. As can be observed in Fig. 7, this coefficient has large negative values for three out of four of the craniums with plagiocephaly and for the cranium with a mixed form of plagiocephaly and brachycephaly (pb1). Furthermore, one cranium with scaphocephaly (sc4) has a comparably low coefficient. For the fourth cranium with plagiocephaly, this coefficient is the highest positive one in comparison to the others. For all other craniums this coefficient is considerably closer to 0. This pattern is observed when the spherical harmonics expansion was performed with an l_{max} of 2,3 and 4, where the plagiocephaly class is most distinguishable from the other classes at

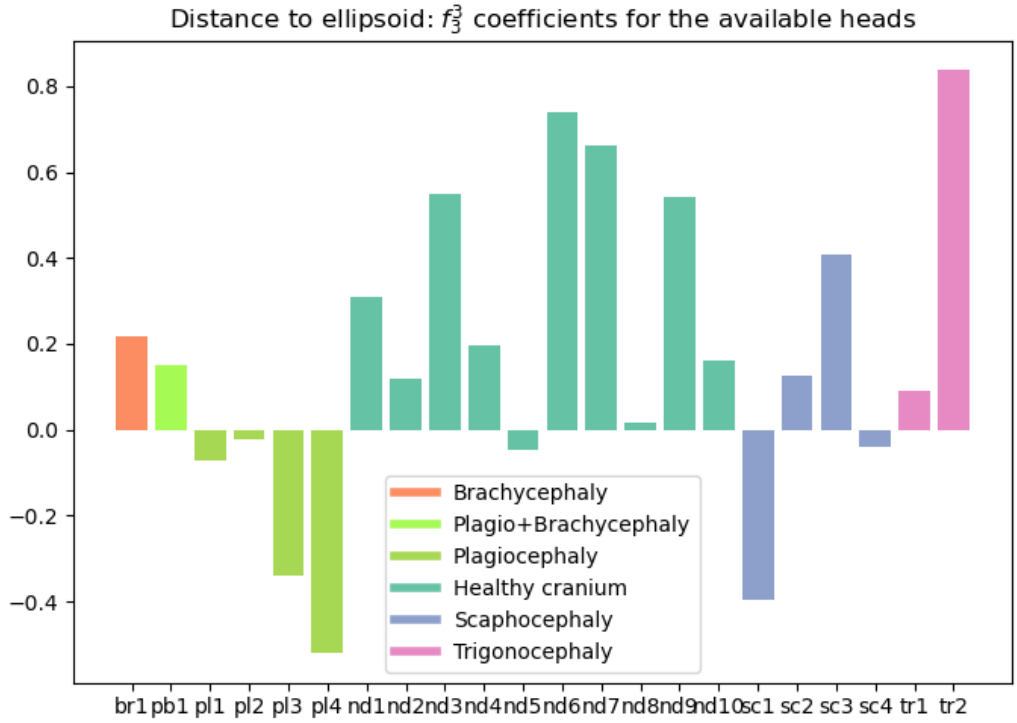

(a) $l_{max} = 3$

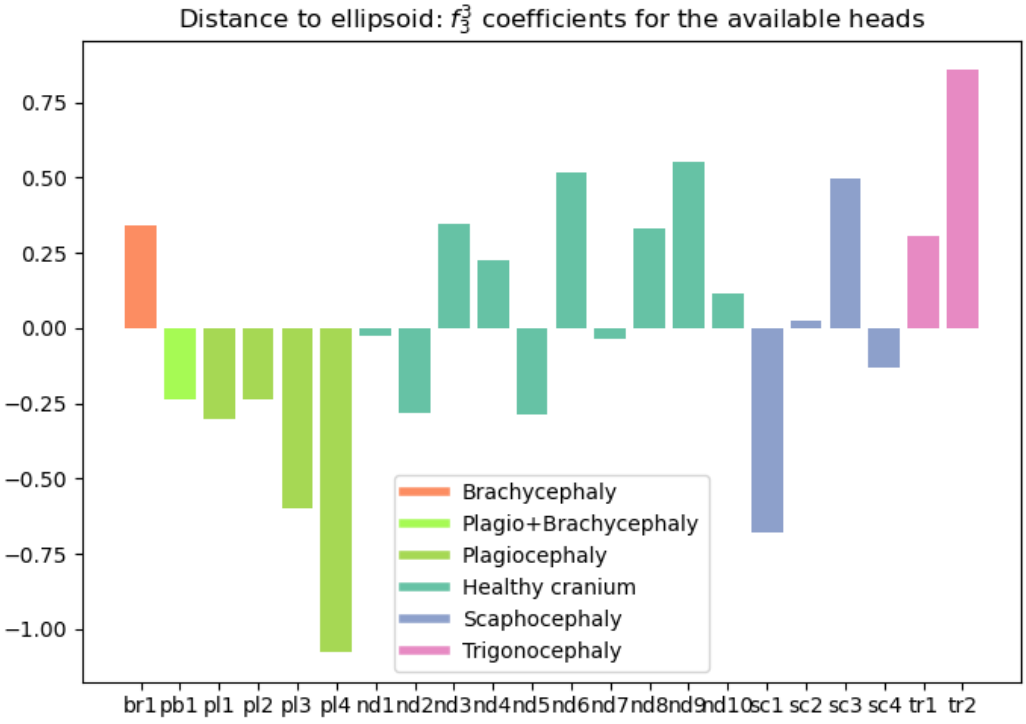

(b) $l_{max} = 4$

Figure 6: The coefficient of degree $l = 3$ and order $m = 3$ for the available heads, in (a) calculated with $l_{max} = 3$, and in (b) calculated with $l_{max} = 4$

$l_{max} = 3$ (Fig. 7a). With an $l_{max} > 4$ this pattern is not observed anymore and the coefficients f_2^{-2} of craniums with plagiocephaly fall in the same range as for the other craniums.

8. Discussion

The results show that the proposed spherical harmonics model is able to model the infant's heads with a high accuracy in relation to the input data, already with low maximum spherical harmonic degrees l_{max}. The error of the model in comparison to the original cranial 3D shape is below 1 mm already under the use of $l_{max} = 4$ and above. This was observed both times, with evaluation of the error at the input vertices and with the evaluation of the distance between both triangle meshes. With an increasing l_{max} the error which is estimated at the input vertices minimizes and converges towards zero, which is expected behavior because the spherical harmonics are actually capable of modeling any arbitrary function on the sphere if the l_{max} is high enough. The higher the degree l, the better is the spherical harmonic able to reproduce small details. However, the created spherical harmonics model should be valid for the whole cranium and not just at the singular points where the input vertices are. This was tested by reconstructing the cranium as triangulated shape based on a regularly sampled spherical grid and evaluating the distance between the original cranial shape and the reconstructed shape. As can be observed in Fig. 4b the error of the spherical harmonics model also decreases towards zero for most of the craniums with an increasing l_{max} up to $l_{max} = 12$. Then, however, the observed error begins to increase again with higher maximum spherical harmonic degrees. This is caused by the fact that the spherical harmonic coefficients are indeed only fitted to match with the punctual input data. In the space between the input points however the value may vary. The higher the degree becomes, the better the coefficients are fitted to the points but the higher becomes the variability in these zones where no data points are. Also the tesselation becomes ever more fine-scaled, which can lead to very high or low values locally.

So while a higher l_{max} minimizes the error measured at the input vertices, it leads to an increasing error in the areas which are not covered by the input vertices from an l_{max} of 12 and upwards. This supports the idea which was formulated at the beginning, that this study must focus on the analysis of the low spherical harmonic degrees. It is logical that for the purpose of this study it is not desirable to model every small detail of the cranium because biologically every head is different and varies in the peculiarity of its details. Furthermore, by modeling every detail with high degree spherical harmonics it is possible that outlier in the input data are thus transferred to the model. As it was mentioned in the beginning, the available triangle meshes of infant's craniums have an accuracy of approximately 2.1 mm, so the information which is represented in the higher spherical harmonic degrees is not reliable. Hence, based on the finding that already with an $l_{max} = 4$ an RMSE of under 1 mm was obtained, the analysis of the spherical harmonic coefficients in order to detect deformations was focused only on the first spherical harmonics up to degree 4.

The best indicator that was found is the coefficient of the spherical harmonic of degree $l = 2$ and order $m = -2$. As it can be appreciated in Fig. 7, the calculated values for this coefficient

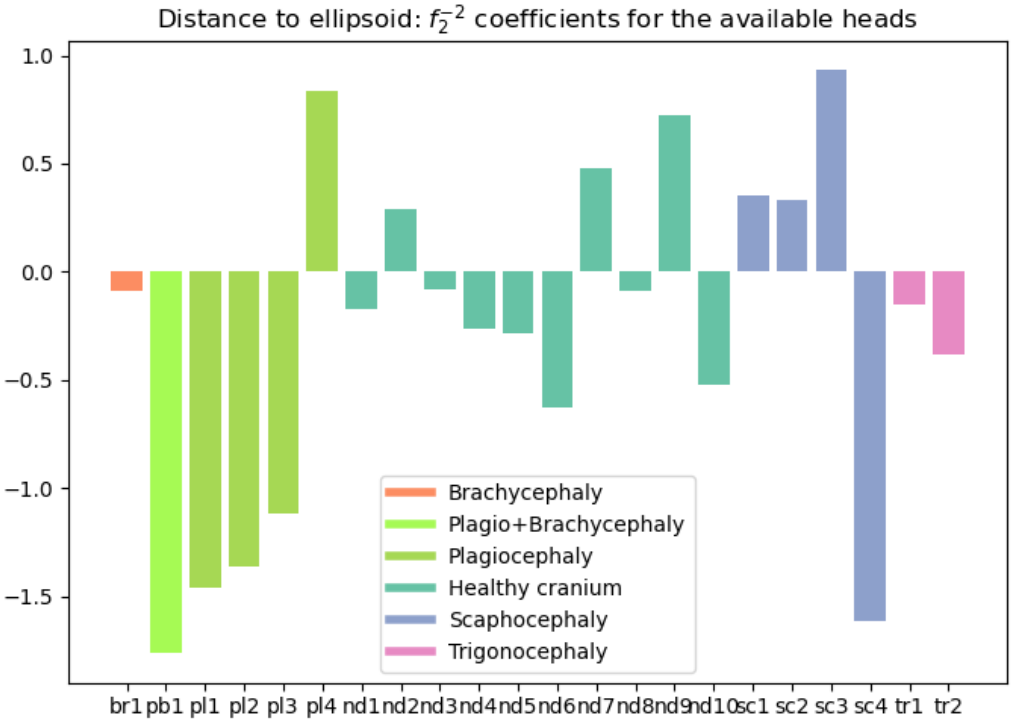

(a) $l_{max} = 3$

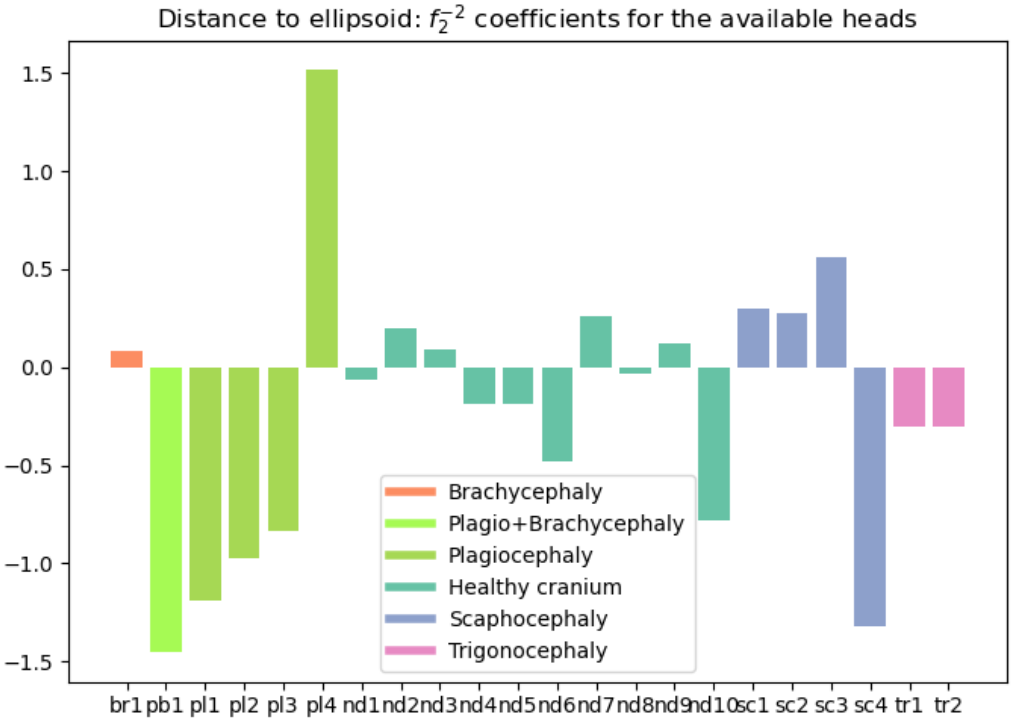

(b) $l_{max} = 4$

Figure 7: The coefficient of degree $l = 2$ and order $m = -2$ for the available heads, in (a) calculated with $l_{max} = 3$, and in (b) calculated with $l_{max} = 4$

are prominently smaller (and in the case of pl4 higher) for the craniums which suffer plagiocephaly than for the other craniums. This means that this specific spherical harmonic has a higher weighting and thus contributes more to the cranial shape for those craniums. The weight of a coefficient is given by its absolute value. So for example, a coefficient of -1.5 represents a higher weight than -0.25. It means that the inverse of the spherical harmonic of degree $l = 2$ and order $m = -2$ contributes well to the model of the cranial shape. This can also be seen as a rotation of 180 degrees of the effect of the spherical harmonic which is shown in Fig. 10. In section 3.2 the idea was presented, that the coefficients f_1^{-1} and f_2^{-2} might serve as indicators for plagiocephaly. It is interesting that for f_2^{-2} this might be the case, meanwhile f_1^{-1} was not found to be meaningful. This means that the resulting coefficients f_1^{-1} for the craniums with plagiocephaly were in the same range as for the other craniums. Apparently, Y_2^{-2} can model the asymmetry caused by plagiocephaly much better than Y_1^{-1}. In Fig. 7 it catches the eye that besides the craniums with plagiocephaly, the cranium *sc4* also has a large weight assigned to f_2^{-2}. *sc4* is a cranium with a strongly elongated head shape. However, despite the fact that the main diagnosis for *sc4* is scaphocephaly, the cranium also has a large, convex bump in the left side of the back of the head (visible in Fig. 15a). This creates a strong asymmetry in the dorsal part of the cranium and thus explains the high weight for this spherical harmonic.

At the beginning of the thesis (in section 3.2), the spherical harmonic of degree $l = 3$ and order $m = 3$ has been suggested as a possible indicator for the detection of trigonocephaly. Based on the results, this can be neither confirmed nor neglected. From the two available craniums with trigonocephaly, *tr1* was assigned a low value for the corresponding coefficient f_3^3 (in the same range as for the other craniums) and *tr2* was assigned a high one. This can be explained by both craniums having a different overall shape even though they have the same type of cranial deformation: While *tr1* has a rather narrow head shape (see Fig. 16, the head shape of *tr2* is broader and with a stronger triangular shape in the forehead (Fig. 17). Thus, the typical triangular shape of *tr2* can be modeled better by the spherical harmonic of degree $l = 3$ and order $m = 3$. Therefore, a high value assigned to the coefficient f_3^3 could be an indicator to detect cranial deformation of the type of trigonocephaly, but maybe it will only be able to detect the severe cases. However, to confirm this assumption more data is necessary: The presented spherical harmonic model needs to be calculated for a larger number of craniums with trigonocephaly and for a control group without trigonocephaly. If the resulting f_3^3 is significantly higher for the craniums with trigonocephaly it can serve as an indicator. This is also supported by the RMSE which was measured for *tr2* between the reconstructed vertices and the original point cloud. As can be seen in Fig. 4a, the RMSE is considerably higher for *tr2* than for all other craniums when the spherical harmonics model was created with $l_{max} = 2$. This means that the spherical harmonics of degree $l = 3$ are necessary to model the cranium well with the spherical harmonic model. However, there is the problem again that this observation is only made for *tr2* but not for *tr1* and more data would be necessary to verify these conclusions. But a possible indicator to detect cranial deformation of the type trigonocephaly could be a combination of the value of the coefficient f_3^3 and the measured RMSE, where a significant decrease in the RMSE from $l_{max} = 2$ to $l_{max} = 3$ would be a sign for trigonocephaly.

Unfortunately, no spherical harmonic Y_l^m, respective its coefficient f_l^m, was found which could serve as an indicator for brachycephaly or scaphocephaly. For none of the analyzed coefficients, the craniums of these two classes showed a specific pattern to discriminate them from the other craniums. This implies that the shape of a cranium with one of these two types of deformations can still be approximated very well with a triaxial ellipsoid. The ellipsoid which is fitted to the cranium might be exceptionally short in the case of brachycephaly, or exceptionally long in the case of scaphocephaly. But the distances from the cranial shape to that ellipsoid are then very similar to the distances from a healthy cranial shape to its best fitted ellipsoid. In contrast, craniums with plagiocephaly and trigonocephaly have a shape which locally differs more from an ellipsoid shape. Plagiocephaly is characterized by an asymmetry in the dorsal part of the head. Therefore, that side of the head which is flattened usually has larger distances to the fitted ellipsoid. And this pattern in the distances is reflected well by the spherical harmonic Y_2^{-2}, which is why it receives a high weight f_2^{-2} in the spherical harmonic model. In the case of trigonocephaly, it is the typical triangular shape of the forehead which is very different to the shape of the ellipsoid. Consequently, the information whether a cranium shows scaphocephaly or brachycephaly should best be given in the length of the axes of the fitted ellipsoid, where the length of the longitudinal axis from the forehead to the back of the head should be compared to the length of the horizontal axis from side to side. However, this is exactly the information which is already measured by the commonly used cephalic index which is given by the ratio between the maximum breadth and the maximum length of the cranium. The cephalic index thus already represents a widely used and standardized method for the effective detection of brachycephaly and scaphocephaly but not for plagiocephaly and trigonocephaly. However, the latter two types of deformation result in a higher and characteristic variation from the surface of the fitted ellipsoid to the cranium, and can thus better be detected with the spherical harmonics model developed in this thesis.

It is disputable whether the constrained rotation that was applied in the fitting of the ellipsoid (section 6.1.1) reflects well the ideal shape of the cranium. In the approach that was implemented in this master thesis, the best fitted ellipsoid is not allowed to be rotated, thus limiting the adjustment parameters to the center and the radii of the axes of the ellipsoid. In contrast, Barbero-García et al. (2017) suggested to constrain only the rotation about the Y-axis, but allowing the rotation of the ellipsoid to be rotated about the other two axes. Of course, the rotation of the ellipsoid has a high influence on the final coefficients f_l^m that are calculated, as it serves as the reference surface for the spherical harmonics. However, when following the approach of Barbero-García et al. (2017) the problem occurred that in some craniums with plagiocephaly the asymmetrical flattening of the back of the head influenced the rotation of the ellipsoid strongly. This is shown in Fig. 8. When the distances to the best fitted ellipsoid are calculated as a global assessment of cranial deformation as in Barbero-García et al. (2017), this does not pose a problem. But for the detection of the cranial deformation with the spherical harmonics this was a problem as it affects the pattern of the distances to the ellipsoid locally. For the aim of this master thesis, it was important that the spherical harmonics which are calculated on the fitted

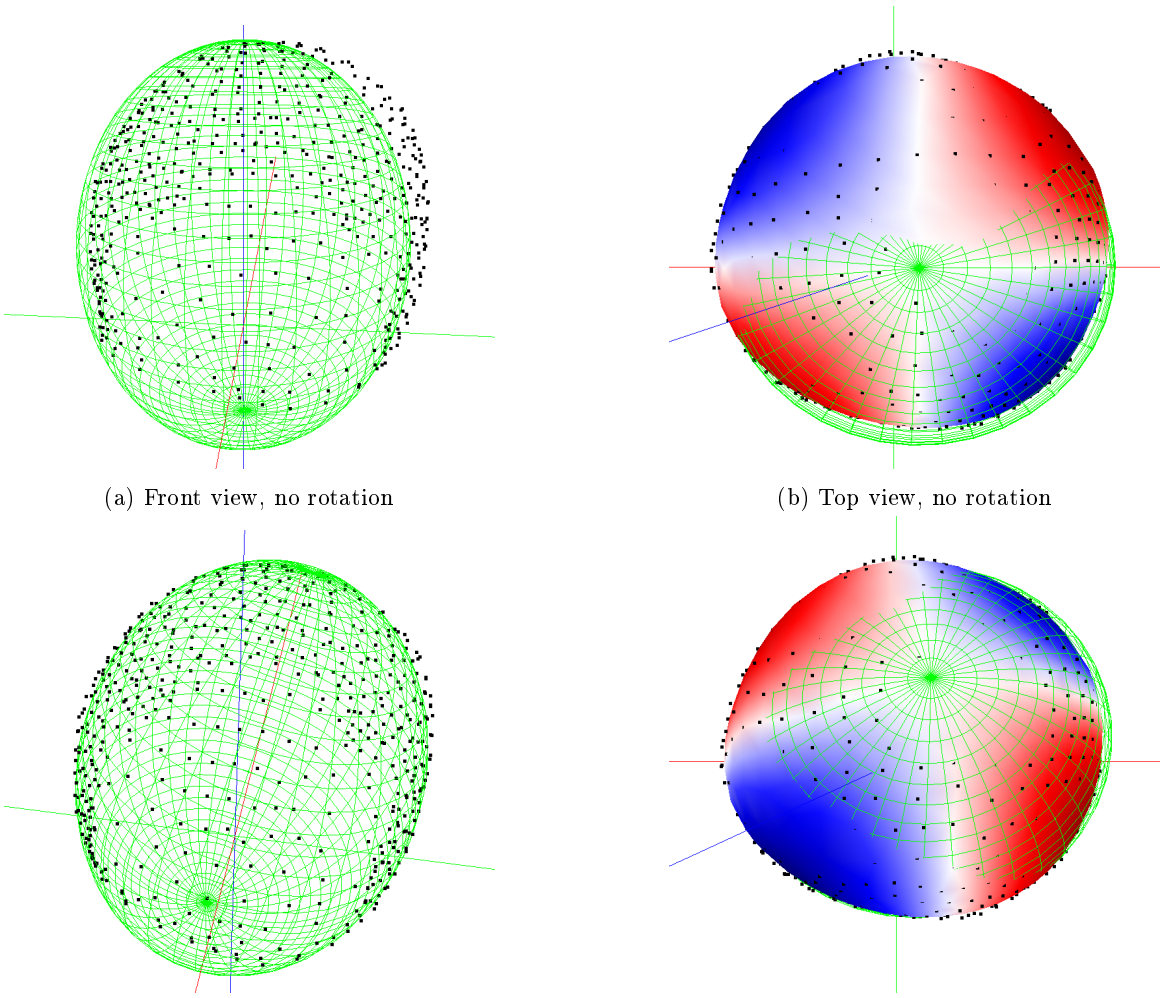

(a) Front view, no rotation

(b) Top view, no rotation

(c) Front view, partly rotation

(d) Top view, partly rotation

Figure 8: Best fitted ellipsoid for the cranium *pl4*: When the rotation is partly allowed as in (c) and (d) the ellipsoid's orientation follows the asymmetry of the plagiocephaly, as a consequence the effect of the spherical harmonic Y_2^{-2} shown in (b) and (d) is altered.

ellipsoid of each cranium are comparable. Therefore, it is important that the ellipsoid is always referenced in relation to the cranium in the same way. With the calculation of the orthogonal distances and assignation to coordinates (θ, ϕ) a "virtual coordinate system" is created on each reference ellipsoid. Only by disabling the rotation of the ellipsoid during the adjustment it could be assured that the "virtual coordinate systems" are always created with the same reference to the cranium, and thus the resulting spherical harmonic coefficients for the different craniums are comparable with each other. In Fig. 9 the mean distance from the craniums to their fitted ellipsoid is shown, where once the rotation of the ellipsoid was constrained as in Barbero-García et al. (2017) and once completely disabled. It can be observed in the figure, that the difference between both approaches is minimal for all craniums except for those with plagiocephaly, where the total distance to the ellipsoid is higher when the rotation of the ellipsoid is disabled.

It is important to note, that the presented results can only be considered as trends. As it has been mentioned various times, more data in the form of 3D cranial models would be necessary to verify the presented results. Unfortunately, only 22 cranial models where available

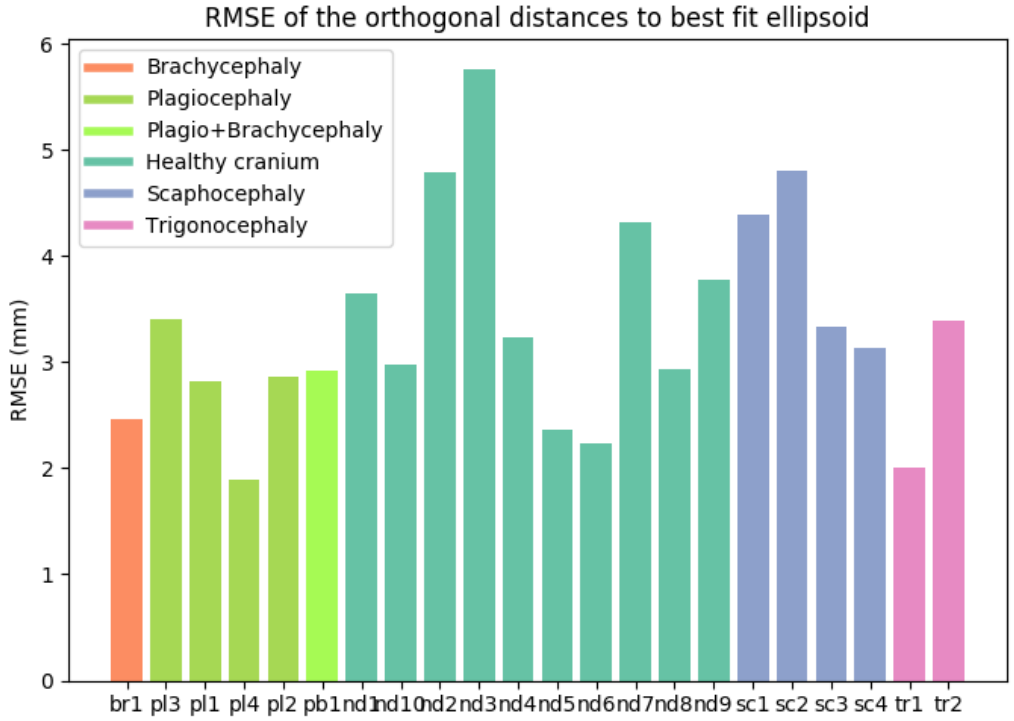

(a)

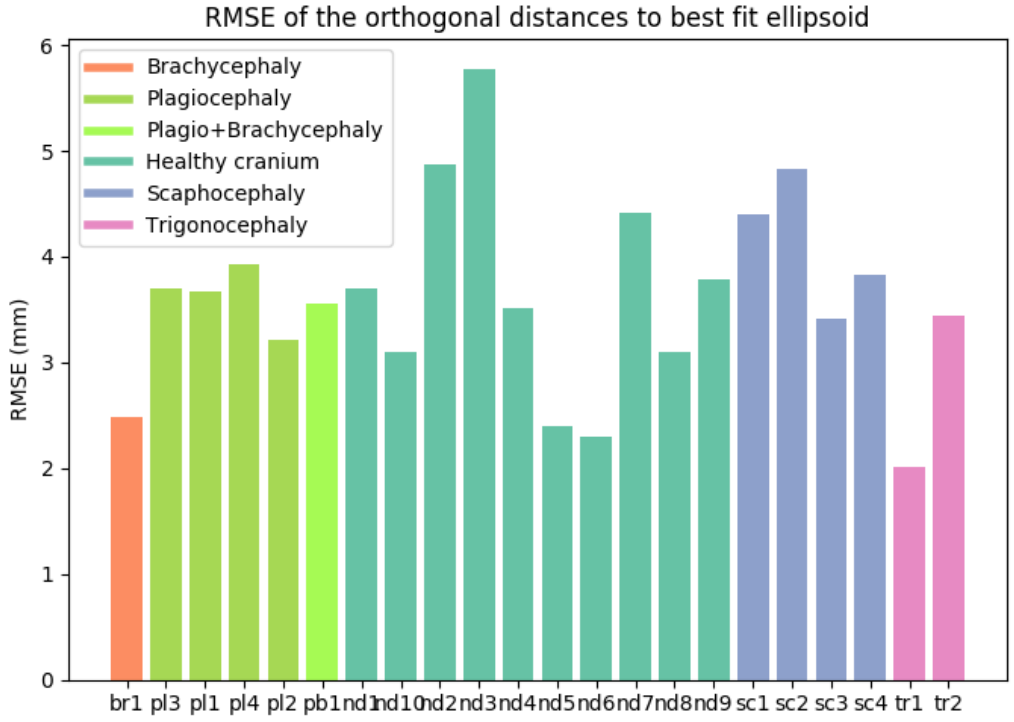

(b)

Figure 9: RMSE of the orthogonal distances to the ellipsoid, where at (a) the ellipsoid was allowed to rotate about the X- and Z-axis, and at (b) the ellipsoid was not rotated

during the realization of the master thesis. No statistical tests could be conducted to test the significance of the results because the size of the sample is too small to be statistically significant. However, with the identification of the coefficients f_2^{-2} and f_3^3 as indicators for plagiocephaly and trigonocephaly, respectively, two important trends have been identified. Furthermore, the main result of the thesis is the implemented spherical harmonics model itself. Since the approach has been designed as an automatized workflow and fully implemented in the Python programming language, it can be easily applied to a larger sample of cranial 3D models, as soon as they are available. Furthermore, when this larger sample is available in the future and the presented spherical harmonics model is calculated for all craniums, more information might be gained: The resulting spherical harmonic coefficients could be analyzed with methods from machine learning (e.g., decision trees, neural networks) in order to detect which coefficients have the highest power to discriminate between the different types of cranial deformation. Subsequently, a classifier can be created which automatically classifies a cranium based on the calculated spherical harmonic coefficients. Finally, this can be used as an automatic method to evaluate infanf's craniums to detect cranial information in combination with the photogrammetry-based creation of 3D models of the cranium as an extension to the routine of infant's health checkups.

9. Conclusion

A method was developed which models the orthogonal distances of a cranium to its best fitted ellipsoid with spherical harmonics. The resulting model is able to approximate the shape of the original 3D model of the cranium with an accuracy of below 1 mm already with a maximum spherical harmonic degree of 4. The resulting coefficients constitute a weighting for the individual spherical harmonics. While these weights can be used as an indicator for plagiocephaly and possibly also for trigonocephaly, the developed approach probably does not support the detection of scaphocephaly and brachycephaly. The coefficient of the spherical harmonic with degree $l = 2$ and order $m = -2$ seems to be the most promising one as an indicator to detect plagiocephaly in infant's craniums. It can also be seen as an indicator for asymmetry in the dorsal part of the cranium. However, to verify this more data is needed. With this data available in the future, the aptness of that specific coefficient as an indicator for plagiocephaly can be tested statistically. More importantly, with more available data the workflow that was developed in this thesis can be applied automatically to all craniums. Then, machine learning methods can be used to create classifiers and thus provide a method for the automatic detection of plagiocephaly in infant's craniums.

References

Aarnivala, H., Vuollo, V., Harila, V., Heikkinen, T., Pirttiniemi, P., Holmström, L., and Valkama, A. M. (2016). The course of positional cranial deformation from 3 to 12 months of age and associated risk factors: a follow-up with 3D imaging. *European Journal of Pediatrics*, 175(12):1893–1903.

Barbero-García, I. and Lerma, J. L. (2019). Assessment of Registration Methods for Cranial 3D Modelling. *Proceedings*, 19(1):8. Number: 1 Publisher: Multidisciplinary Digital Publishing Institute.

Barbero-García, I., Lerma, J. L., and Marqués-Mateu, A. (2017). Low-Cost Smartphone-Based Photogrammetry for the Analysis of Cranial Deformation in Infants. *World Neurosurgery*, 102:545–554.

Barbero-García, I., Lerma, J. L., Miranda, P., and Marqués Mateu, A. (2019). Smartphone-based photogrammetric 3D modelling assessment by comparison with radiological medical imaging for cranial deformation analysis. *Measurement*, 131:372–379.

Bektas, S. (2014). Orthogonal distance from an ellipsoid. *Boletim de Ciencias Geodesicas*, 20(4):970–983.

Bektas, S. (2015). Least squares fitting of ellipsoid using orthogonal distances. *Boletim de Ciências Geodésicas*, 21(2):329–339.

Boulet, S. L., Rasmussen, S. A., and Honein, M. A. (2008). A population-based study of craniosynostosis in metropolitan Atlanta, 1989–2003. *American Journal of Medical Genetics Part A*, 146A(8):984–991. _eprint: https://onlinelibrary.wiley.com/doi/pdf/10.1002/ajmg.a.32208.

Ducroz, C., Olivo-Marin, J.-C., and Dufour, A. (2012). Characterization of cell shape and deformation in 3D using Spherical Harmonics. In *2012 9th IEEE International Symposium on Biomedical Imaging (ISBI)*, pages 848–851. ISSN: 1945-8452.

El-Baz, A., Nitzken, M., Elnakib, A., Khalifa, F., Gimel'farb, G., Falk, R., and El-Ghar, M. A. (2011). 3D shape analysis for early diagnosis of malignant lung nodules. *Medical image computing and computer-assisted intervention: MICCAI ... International Conference on Medical Image Computing and Computer-Assisted Intervention*, 14(Pt 3):175–182.

Gerig, G., Styner, M., Jones, D., Weinberger, D., and Lieberman, J. (2001). Shape analysis of brain ventricles using SPHARM. In *Proceedings IEEE Workshop on Mathematical Methods in Biomedical Image Analysis (MMBIA 2001)*, pages 171–178.

Ho, O. A., Saber, N., Stephens, D., Clausen, A., Drake, J., Forrest, C., and Phillips, J. (2017). Comparing the Use of 3D Photogrammetry and Computed Tomography in Assessing the Severity of Single-Suture Nonsyndromic Craniosynostosis. *Plastic Surgery*, 25(2):78–83.

Johnson, D. and Wilkie, A. O. M. (2011). Craniosynostosis. *European Journal of Human Genetics*, 19(4):369–376.

Judd, T. (2020). 3D Ellipsoid, Best Fit. Retrieved May 13, 2020, from `http://www.juddzone.com/ALGORITHMS/least_squares_3D_ellipsoid.html`.

Kakarala, R., Kaliamoorthi, P., and Premachandran, V. (2013). Three-Dimensional Bilateral Symmetry Plane Estimation in the Phase Domain. In *2013 IEEE Conference on Computer Vision and Pattern Recognition*, pages 249–256, Portland, OR, USA. IEEE.

Lerma, J. L., Barbero-García, I., Marqués-Mateu, A., and Miranda, P. (2018). Smartphone-based video for 3D modelling: Application to infant's cranial deformation analysis. *Measurement*, 116:299–306.

Ligas, M. (2012). Cartesian to geodetic coordinates conversion on a triaxial ellipsoid. *Journal of Geodesy*, 86(4):249–256.

Mehta, V. A., Bettegowda, C., Jallo, G. I., and Ahn, E. S. (2010). The evolution of surgical management for craniosynostosis. *Neurosurgical Focus*, 29(6):E5. Publisher: American Association of Neurological Surgeons.

Meulstee, J. W., Verhamme, L. M., Borstlap, W. A., Van der Heijden, F., De Jong, G. A., Xi, T., Bergé, S. J., Delye, H., and Maal, T. J. J. (2017). A new method for three-dimensional evaluation of the cranial shape and the automatic identification of craniosynostosis using 3D stereophotogrammetry. *International Journal of Oral and Maxillofacial Surgery*, 46(7):819–826.

Miller, R. I. and Clarren, S. K. (2000). Long-Term Developmental Outcomes in Patients With Deformational Plagiocephaly. *PEDIATRICS*, 105(2):e26–e26.

Pavlis, N. K., Holmes, S. A., Kenyon, S. C., and Factor, J. K. (2012). The development and evaluation of the Earth Gravitational Model 2008 (EGM2008). *Journal of Geophysical Research: Solid Earth*, 117(B4). _eprint: https://agupubs.onlinelibrary.wiley.com/doi/pdf/10.1029/2011JB008916.

Pindrik, J., Molenda, J., Uribe-Cardenas, R., Dorafshar, A. H., and Ahn, E. S. (2016). Normative ranges of anthropometric cranial indices and metopic suture closure during infancy. *Journal of Neurosurgery: Pediatrics*, 18(6):667–673.

Roth, S. D. (1982). Ray casting for modeling solids. *Computer Graphics and Image Processing*, 18(2):109–144.

Schaaf, H., Wilbrand, J.-F., Boedeker, R.-H., and Howaldt, H.-P. (2010). Accuracy of Photographic Assessment Compared with Standard Anthropometric Measurements in Nonsynostotic Cranial Deformities. *The Cleft Palate-Craniofacial Journal*, 47(5):447–453. Publisher: SAGE Publications.

Vuollo, V., Holmström, L., Aarnivala, H., Harila, V., Heikkinen, T., Pirttiniemi, P., and Valkama, A. M. (2016). Analyzing infant head flatness and asymmetry using kernel density estimation of directional surface data from a craniofacial 3D model. *Statistics in Medicine*, 35(26):4891–4904. _eprint: https://onlinelibrary.wiley.com/doi/pdf/10.1002/sim.7032.

Wieczorek, M. A. and Meschede, M. (2018). SHTools: Tools for Working with Spherical Harmonics. *Geochemistry, Geophysics, Geosystems*, 19(8):2574–2592.

Wong, J. Y., Oh, A. K., Ohta, E., Hunt, A. T., Rogers, G. F., Mulliken, J. B., and Deutsch, C. K. (2008). Validity and Reliability of Craniofacial Anthropometric Measurement of 3D Digital Photogrammetric Images. *The Cleft Palate-Craniofacial Journal*, 45(3):232–239.

A. Appendix

A.1. Programming code

A.1.1. Calculate the best fit ellipsoid

```
def bestFitEllipsoid(pntCloud):
    # This function is adapted and modified from Judd (2020)
    # pntCloud as an array of points with the shape n x 3
    # reshape points to get all x,y,z as independent arrays
    x = pntCloud[:,0][:,np.newaxis]
    y = pntCloud[:,1][:,np.newaxis]
    z = pntCloud[:,2][:,np.newaxis]
    #  Ax^2 + By^2 + Cz^2 +  Dxy +  Exz +  Fyz +  Gx +  Hy +  Iz = 1
    J = np.hstack((x*x,y*y,z*z,x*y,x*z,y*z, x, y, z))
    K = np.ones_like(x)
    JT=J.transpose()
    JTJ = np.dot(JT,J)
    InvJTJ=np.linalg.inv(JTJ);
    ABC= np.dot(InvJTJ, np.dot(JT,K))
    polyn=np.append(ABC,-1)
    # Set D,E,F to 0 to completely constrain the rotation
    polyn[3], polyn[4], polyn[5] = 0,0,0
    # Now we need to extract the parameters from the polynomial solution
    Amatrix=np.array([
        [ polyn[0],     polyn[3]/2.0, polyn[4]/2.0, polyn[6]/2.0 ],
        [ polyn[3]/2.0, polyn[1],     polyn[5]/2.0, polyn[7]/2.0 ],
        [ polyn[4]/2.0, polyn[5]/2.0, polyn[2],     polyn[8]/2.0 ],
        [ polyn[6]/2.0, polyn[7]/2.0, polyn[8]/2.0, polyn[9]     ]
        ])
    A3=Amatrix[0:3,0:3]
    # Extract the center
    A3inv=np.linalg.inv(A3)
    ofs=polyn[6:9]/2.0
    center=-np.dot(A3inv,ofs)
    # Extract the axes radii and the rotation as a rotation matrix
    Tofs=np.eye(4)
    Tofs[3,0:3]=center
    R = np.dot(Tofs,np.dot(Amatrix,Tofs.T))
    R3=R[0:3,0:3]
    R3test=R3/R3[0,0]
    s1=-R[3, 3]
    R3S=R3/s1
    (el,ec)=np.linalg.eig(R3S)
    recip=1.0/np.abs(el)
    axes=np.sqrt(recip)
    inve=np.linalg.inv(ec)
    return (center,axes,inve)
```

A.1.2. Extraction of the orthogonal distances to the ellipsoid

```
def orthogonalDistancesToEllipsoid(pntCloud, axisradii):
    # pntCloud as an array of points with the shape N x 3
    ax, ay, b = axisradii
    e = 1/(ax*ax)
    f = 1/(ay*ay)
    g = 1/(b*b)

    phis = []
    thetas = []
    distances = []
    pntsOnEllip = []

    for pnt in pntCloud:
        xg,yg,zg = pnt
        x0 = (ax*xg)/np.linalg.norm(pnt)
        y0 = (ay*yg)/np.linalg.norm(pnt)
        z0 = (b*zg)/np.linalg.norm(pnt)

        # Xe is the first guess of the closest point
        Xe = np.array([[x0],[y0],[z0]])
        j = 0
        # iteratively improve Xe
        while True:
            x0,y0,z0 = [i[0] for i in Xe]

            j11 = f*y0 - (y0-yg)*e
            j12 = (x0-xg)*f-e*x0
            j13 = 0
            j21 = g*z0-(z0-zg)*e
            j22 = 0
            j23 = (x0-xg)*g-e*x0
            j31 = 2*e*x0
            j32 = 2*f*y0
            j33 = 2*g*z0

            A = np.array([
                [j11, j12, j13],
                [j21, j22, j23],
                [j31, j32, j33]
            ])

            f1 = (x0-xg)*f*y0-(y0-yg)*e*x0
            f2 = (x0-xg)*g*z0-(z0-zg)*e*x0
            f3 = e*x0*x0+f*y0*y0+g*z0*z0-1

            df = np.array([[f1],[f2],[f3]])
            diff = np.linalg.solve(-A,df)
```

```
48              Xe = Xe + diff
49
50              # Stopping criterion
51              if np.sum(np.abs(diff)) < 0.5 or j > 15:
52                  break
53              j += 1
54
55          # Closest point is found, now calculate orthogonal distance
56          distance = np.linalg.norm(pnt-Xe.T[0])
57          # Check if original point is within Ellipsoid
58          # If true, store a negative distance
59          x,y,z = pnt
60          ellipValue = (x*x)/(ax*ax)+(y*y)/(ay*ay)+(z*z)/(b*b)
61          if ellipValue < 1:
62              distance *= -1
63
64          xe,ye,ze = Xe.T[0]
65          pntsOnEllip.append(Xe.T[0])
66
67          # convert Xe from Cartesian to spherical coordinates
68          phi, theta = cartesianToEllipCoord(xe, ye, ze, axisradii)
69          phis.append(phi)
70          thetas.append(theta)
71          distances.append(distance)
72
73      distances = np.array(distances)
74      phis = np.array(phis)
75      thetas = np.array(thetas)
76      return (distances, phis, thetas, pntsOnEllip)
```

A.1.3. Coordinate conversion on the ellipsoid

```
def cartesianToEllipCoord(x, y, z, axesradii):
    # Converts the cartesian coordinate given by x,y,z to the spherical
    # coordinate (phi, theta) on the triaxial ellipsoid which is
    # defined by the axesradii.
    # Method according to Ligas (2012)
    # Returns phi as latitude and theta as longitude value
    ax, ay, b = axesradii
    ecc_x2 = (ax*ax - b*b)/(ax*ax)
    ecc_e2 = (ax*ax - ay*ay)/(ax*ax)

    divisor = np.sqrt(np.power(1-ecc_e2,2)*np.power(x,2)+np.power(y,2))
    phi = np.arctan(((1-ecc_e2)/(1-ecc_x2))*(z/divisor))
    theta = np.arctan((1/(1-ecc_e2))*(y/x))
    if x < 0:
        theta = -np.pi + theta
    return (phi, theta)


def ellipToCartesianCoord(phi, theta, axesradii):
    # Converts the spherical coordinate given by (phi, theta) to
    # a Cartesian coordinate on the ellipsoid defined by the axesradii.
    # phi as the latitude, theta as longitude, both in radians
    ax, ay, b = axesradii
    ecc_x2 = (ax*ax - b*b)/(ax*ax)
    ecc_e2 = (ax*ax - ay*ay)/(ax*ax)
    divisor = np.sqrt(1-ecc_x2*np.power(np.sin(phi),2)-ecc_e2*np.power(
            np.cos(phi),2)*np.power(np.sin(theta),2))
    curv = ax/divisor

    x = curv * np.cos(phi) * np.cos(theta)
    y = curv * (1-ecc_e2)*np.cos(phi)*np.sin(theta)
    z = curv * (1-ecc_x2)*np.sin(phi)

    return np.array([x, y, z])
```

A.1.4. Calculation of the spherical harmonic coefficients and reconstruction of the points

```
def transformPoints(pnts, center, rotationMatrix):
    pnts_transformed = []
    for p in pnts:
        pnts_transformed.append(rotationMatrix.dot(p - center))
    return np.array(pnts_transformed)

def retransformPoints(pnts, center, rotationMatrix):
    pnts_transformed = []
    for p in pnts:
        pnts_transformed.append(rotationMatrix.T.dot(p) + center)
    return np.array(pnts_transformed)

def addOrthogonalDistance(pnt, axesradii, distance):
    x, y, z = pnt
    a, b, c = axesradii
    gradient = 2*np.array([x/(a*a), y/(b*b), z/(c*c)])
    unit_vector = gradient / np.linalg.norm(gradient)
    return pnt + unit_vector*distance

def modelSH(pathToPlyModel, lmax):
    head_mesh = o3d.io.read_triangle_mesh(pathToPlyModel)
    headPnts = np.asarray(head_mesh.vertices)

    # Calculate the best fit ellipsoid
    bestFitEllipsoid = bestFitEllipsoid(headPnts)
    center, axesradii, rotationMatrix = bestFitEllipsoid
    # Transform the original point cloud (translation and rotation
    # so that it is in the same reference system as the ellipsoid
    headPnts_rotated = transformPoints(headPnts, center, rotationMatrix)
    # Calculate the orthogonal distances and the coordinates on the ellipsoid
    distances, phis, thetas, pntsOnEllip = \
            orthogonalDistancesToEllipsoid(headPnts_rotated, axesradii)

    latitudes = np.degrees(phis)
    longitudes = np.degrees(thetas)
    cilm, chi = pyshtools.expand.SHExpandLSQ(distances, latitudes, longitudes, lmax)
    coefficients = pyshtools.SHCoeffs.from_array(cilm)

    # Reconstruction of the original point cloud:
    # Estimate the distances based on the spherical harmonic coefficients
    estimated_distances_sh = coefficients.expand(lat=latitudes, lon=longitudes)
    estimated_points_sh = []
    for i in range(len(phis)):
        pntOnEllipsoid = ellipToCartesianCoord(phis[i], thetas[i], axesradii)
        pntEstimated = addOrthogonalDistance(pntOnEllipsoid,
                axesradii, estimated_distances_sh[i])
        estimated_points_sh.append(pntEstimated)
```

```
48
49      # Retransform the points by shifting it to the original center
50      # and multiplication with the inverse rotation matrix so that
51      # the reconstructed points are in the same system as the original head points
52      pnts_reconstructed = retransformPoints(estimated_points_sh, center, rotationMatrix
53      # Calculate the distance between every original point and the reconstructed one
54      distances = []
55      for pnt_orig, pnt_sh in zip(headPnts, pnts_reconstructed):
56          distances.append(np.linalg.norm(pnt_orig - pnt_sh))
57      distances = np.array(distances)
58      rmse =  np.sqrt((distances **2).mean())
```

A.1.5. Create a regular sample of points which form a sphere

This function creates a set of *n_sample* points in spherical coordinates which form a unit sphere, where the values in the array *phi* represent the height angles (as colatitudes, in radians) and the values in the array *theta* represent the corresponding azimuth angles (in radians). The resulting points are not an equidistant sample on the sphere after converting them to the Cartesian space: close to the poles the sampled points are closer and close to the equator the distances between the points are larger.

```
1  def getSample(n_sample):
2      # Create a unit sphere with the resolution of "n_sample"
3      phi = np.linspace(0, np.pi, n_sample)
4      theta = np.linspace(0, 2*np.pi, n_sample)
5      phi, theta = np.meshgrid(phi, theta)
6      return (theta.flatten(), phi.flatten())
```

A.2. Spherical harmonic functions visualized on a cranium

The function values of all spherical harmonics up to degree $l = 3$ and order $m = 3$ have been calculated and are displayed on an example cranium (corresponding to the upper half of the sphere), excluding the function of order $m = 0$. The resulting values were normalized to the range $[-1; +1]$ and visualized on the surface of the 3D model of the cranium. Red symbolizes positive function values and blue negative values. The used 3D model is sc5. The left image always shows the right side view on the cranium and the right image the top view on the cranium.

Degree 1

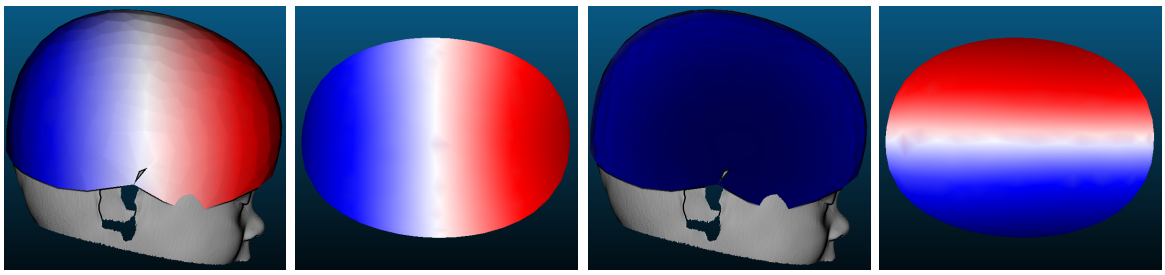

(a) $l = 1, m = 1$ (b) $l = 1, m = -1$

Degree 2

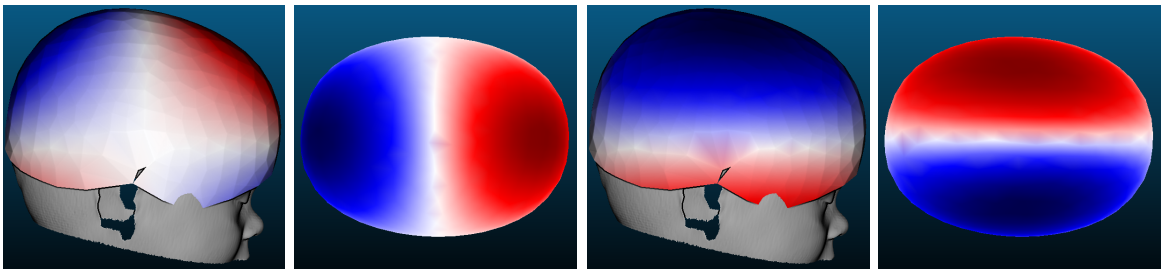

(c) $l = 2, m = 1$ (d) $l = 2, m = -1$

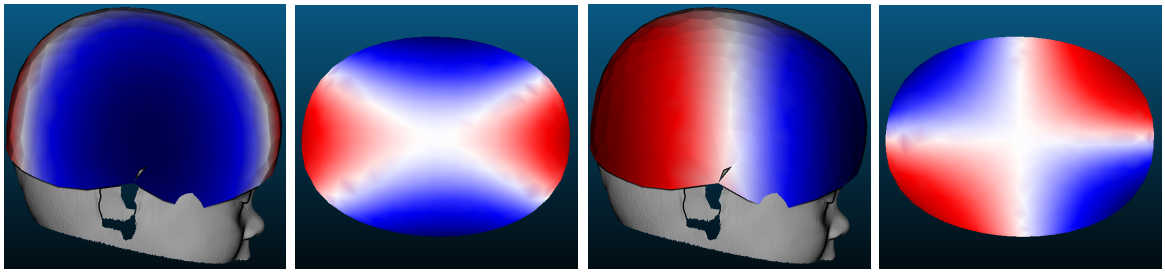

(e) $l = 2, m = 2$ (f) $l = 2, m = -2$

Figure 10: Visualization of spherical harmonic functions of degree 1 and 2

Degree 3

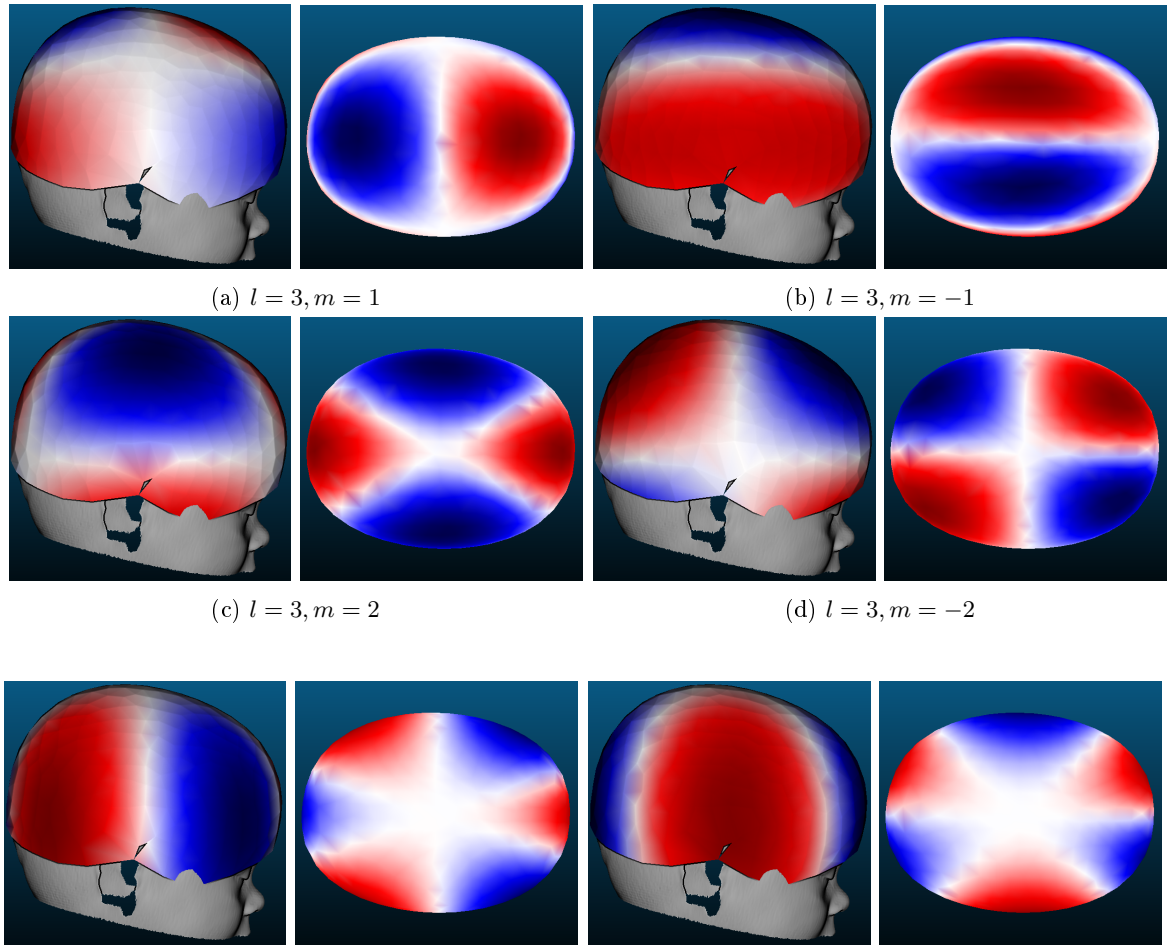

(a) $l = 3, m = 1$ (b) $l = 3, m = -1$

(c) $l = 3, m = 2$ (d) $l = 3, m = -2$

(e) $l = 3, m = 3$ (f) $l = 3, m = -3$

Figure 11: Visualization of spherical harmonic functions of degree 3

A.3. Visualization of the orthogonal distances to the ellipsoid on examplary craniums

In the following, the orthogonal distances to the ellipsoid will be visualized on some of the available craniums. The ellipsoid was calculated as the best fitted ellipsoid without rotation. For each type of cranial deformation and for the group of healthy craniums in the available data, one to two examples will be shown. The orthogonal distances are visualized with colors, where a deep blue means that the orthogonal distance to the ellipsoid is high and the cranial surface is inside the fitted ellipsoid at this position. Areas colored in deep red also show high orthogonal distances but they are outside of the ellipsoid. The fitted ellipsoid for each cranium is shown in green. In each figure, (a) shows the top view on the head which faces towards the right side, (b) shows the right side where the head also faces towards the right and (c) shows the left side of the head with the face towards the left.

Brachycephaly

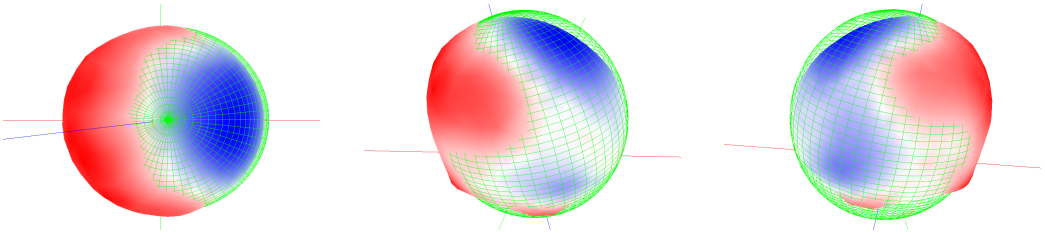

(a) (b) (c)

Figure 12: Visualization of the orthogonal distances to the fitted ellipsoid for the cranium with the id br1

Plagiocephaly

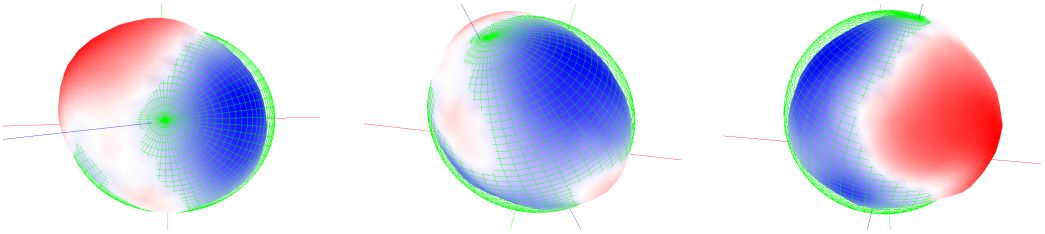

(a) (b) (c)

Figure 13: Visualization of the orthogonal distances to the fitted ellipsoid for the cranium with the id pl1

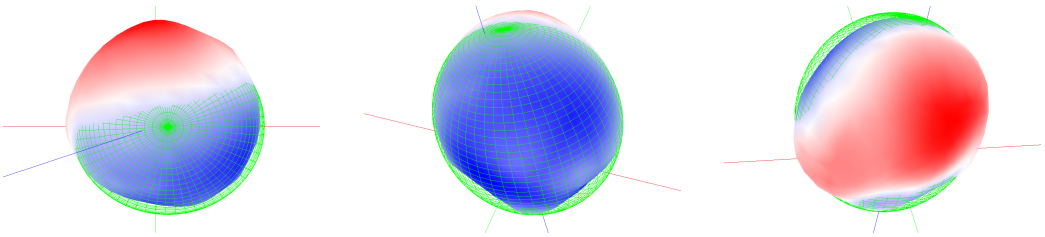

(a) (b) (c)

Figure 14: Visualization of the orthogonal distances to the fitted ellipsoid for the cranium with the id pl4

Scaphocephaly

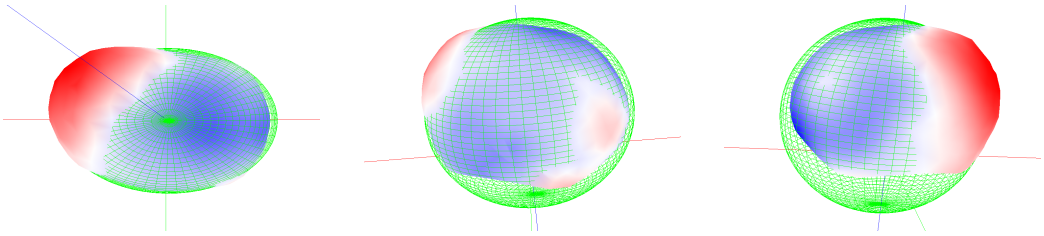

(a) (b) (c)

Figure 15: Visualization of the orthogonal distances to the fitted ellipsoid for the cranium with the id sc4

Trigonocephaly

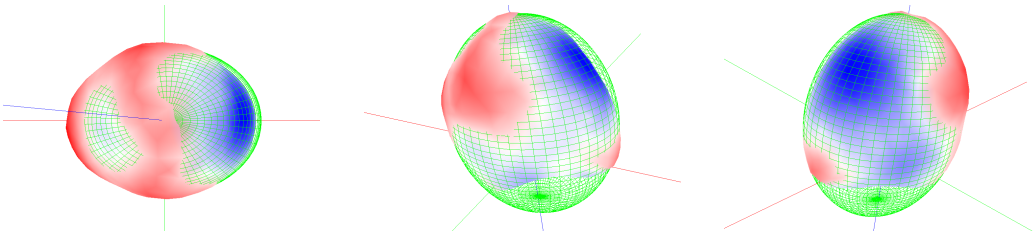

(a) (b) (c)

Figure 16: Visualization of the orthogonal distances to the fitted ellipsoid for the cranium with the id tr1

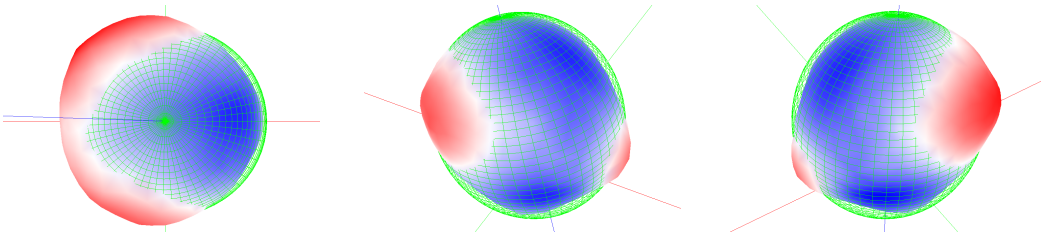

(a) (b) (c)

Figure 17: Visualization of the orthogonal distances to the fitted ellipsoid for the cranium with the id tr2

No deformation

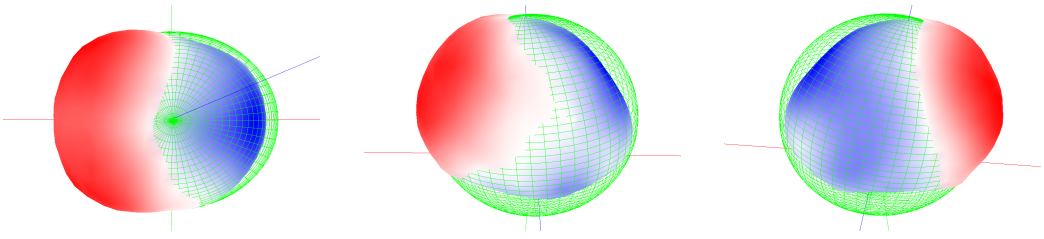

(a) (b) (c)

Figure 18: Visualization of the orthogonal distances to the fitted ellipsoid for the cranium with the id nd3

A.4. Calculated coefficients for lmax=4

ID	l0m0	l1m0	l1m1	l1m-1	l2m0	l2m1	l2m-1	l2m2	l2m-2
br1	9.09	-13.25	-3.33	-0.4	10.17	1.59	0.18	0.11	0.08
pb1	3.94	-5.43	-5.86	0.43	2.5	4.11	0.05	1.51	-1.45
pl1	5.84	-8.15	-4.77	0.52	5.53	2.87	0.68	1.38	-1.19
pl2	7.38	-10.22	-4.49	-0.7	7.17	2.39	0.58	1.53	-0.97
pl3	11.93	-16.44	-6.92	-0.38	12.35	4.48	0.56	1.18	-0.83
pl4	17.24	-22.7	-10	0.21	16.11	11.6	3.75	2.52	1.52
nd1	5.65	-9.04	-5.04	-0.47	6.42	2.6	-0.09	0.84	-0.06
nd10	4.35	-6.74	-4.01	0.45	4.64	1.88	-2.11	0.44	-0.78
nd2	1.52	-1.59	-5.4	0.52	0.71	0.75	0.31	1.08	0.2
nd3	-7.24	10.21	-3.55	-0.08	-7.63	-2.47	-0.38	0.19	0.09
nd4	6.03	-8.75	-3.02	-0.24	6.92	-0.17	1.76	-0.39	-0.19
nd5	4.24	-6	-3.43	0.14	5.03	1.97	-0.29	-0.42	-0.18
nd6	-5.83	7.59	2.02	-1.72	-6.49	-2.76	2.33	0	-0.48
nd7	4.7	-7.01	-5.17	-0.35	4.25	1.06	-0.13	1.79	0.26
nd8	-5.26	5.06	0.04	1.41	-3.37	-2.79	-0.97	-0.49	-0.03
nd9	2.95	-4.71	-3.61	0.72	3.81	0.52	-0.69	0.17	0.12
sc1	2.23	-4.29	-5.85	-0.16	1.79	1.09	-0.03	0.78	0.3
sc2	7.13	-11.6	-5.46	0.27	8.42	0.61	0.13	0.44	0.27
sc3	1.38	-3.01	-2.97	0.25	1.69	0.33	-0.17	0.48	0.56
sc4	5.97	-9.09	-2.86	1.11	8.09	-0.01	-0.17	-1.64	-1.32
tr1	6.78	-9.94	-2.29	0.41	8.47	1.16	-0.65	-0.27	-0.3
tr2	10.07	-15.06	-2.45	0.13	12.67	0.5	0.15	0.67	-0.3

ID	l3m0	l3m1	l3m-1	l3m2	l3m-2	l3m3	l3m-3	l4m0
br1	-5.83	-2.68	-0.22	-0.30	-0.25	0.34	0.04	1.30
pb1	-0.86	-3.93	0.37	-2.10	-0.30	-0.24	0.35	-0.32
pl1	-2.85	-3.11	-0.02	-2.16	-0.46	-0.30	0.03	0.69
pl2	-3.74	-2.65	-0.37	-2.14	-0.63	-0.24	0.37	0.83
pl3	-6.47	-4.84	-0.35	-1.45	-0.34	-0.60	0.05	1.84
pl4	-7.60	-8.59	-1.77	-3.11	-1.57	-1.08	-0.15	1.80
nd1	-4.07	-3.78	0.01	-1.44	0.09	-0.03	0.14	1.23
nd10	-2.49	-2.73	1.31	-0.93	0.30	0.12	0.05	0.27
nd2	-0.51	-2.57	0.07	-1.51	0.22	-0.28	-0.10	-0.31
nd3	3.24	-1.16	0.31	-0.47	-0.42	0.35	0.15	-1.14
nd4	-4.56	-1.77	-1.10	0.19	-0.30	0.22	0.02	1.12
nd5	-3.27	-2.46	0.22	0.55	0.07	-0.28	-0.04	0.47
nd6	3.28	0.36	-1.88	-0.28	0.14	0.52	-0.26	-0.82
nd7	-2.65	-2.41	-0.08	-2.55	0.28	-0.03	0.22	0.45
nd8	0.32	0.21	0.89	-0.19	-0.21	0.33	0.07	0.07

ID	l3m0	l3m1	l3m-1	l3m2	l3m-2	l3m3	l3m-3	l4m0
nd9	-2.67	-2.25	0.52	-0.68	0.82	0.55	-0.01	1.08
sc1	-0.91	-2.76	0.04	-1.29	-0.17	-0.68	-0.11	-0.28
sc2	-5.57	-3.08	-0.07	-0.95	-0.02	0.03	-0.18	1.33
sc3	-1.31	-2.03	0.12	-1.66	-0.10	0.50	0.10	0.42
sc4	-5.70	-1.57	0.87	1.80	-0.36	-0.13	0.02	0.92
tr1	-5.06	-1.87	0.52	-0.35	0.16	0.30	-0.12	2.22
tr2	-8.69	-1.63	-0.08	-1.43	-0.18	0.86	0.21	2.51

ID	l4m1	l4m-1	l4m2	l4m-2	l4m3	l4m-3	l4m4	l4m-4
br1	0.69	0.11	-0.34	0.24	-0.22	0.08	0	-0.05
pb1	0.88	-0.39	-0.01	0.33	0.57	0.21	0.05	-0.11
pl1	0.98	-0.41	0.03	0.29	0.44	0.12	-0.09	0
pl2	0.83	0.19	0.23	0.47	0.3	0.14	0.16	-0.08
pl3	1.58	-0.01	0.26	0.33	0.47	0.14	-0.09	-0.06
pl4	3.16	0.45	0.78	0.56	0.67	-0.23	0.01	0.26
nd1	1.07	0.2	-0.6	0.05	0.88	0.16	0.03	-0.02
nd10	1.71	-0.79	0.24	-0.24	0.14	0.08	-0.24	0.04
nd2	0.76	-0.02	-0.01	-0.08	0.91	-0.19	-0.3	0.01
nd3	0.63	0.08	-0.45	0.11	0.46	0.22	-0.76	0.26
nd4	0.21	0.13	-1.04	0.07	0	-0.18	-0.1	0.07
nd5	0.29	0.05	0.1	0.02	0.53	-0.12	-0.58	0.2
nd6	-0.99	0.96	-0.65	0.14	0.42	0.08	-0.06	0.02
nd7	0.47	0.24	0	-0.12	0.83	-0.1	0.1	-0.09
nd8	0.98	-0.73	-0.58	0.08	-0.34	0.02	0.02	-0.07
nd9	1.25	-0.32	-0.59	-0.58	0.17	-0.12	-0.08	-0.01
sc1	0.64	-0.05	0.08	-0.02	0.64	0.17	-0.41	-0.17
sc2	1.23	-0.16	-0.36	-0.1	0.41	-0.14	-0.27	-0.01
sc3	1.17	-0.16	-0.22	-0.26	0.12	-0.03	-0.28	-0.29
sc4	0.55	-0.57	-0.43	0.09	0.19	0.63	-0.76	0.45
tr1	1.44	-0.03	-0.73	-0.18	-0.51	-0.11	0.14	0.09
tr2	1.06	-0.1	-0.22	0.14	-0.05	0.03	0.37	0.02